

Application and Evaluation of CRACMM V1.0 Mechanism in PM_{2.5} Simulation Over China

Qingfang Su¹, Yifei Chen¹, Yangjun Wang^{1*}, David C. Wong^{2,3}, Havala O. T. Pye², Ling Huang¹, Golam Sarwar², Benjamin Murphy², Bryan Place⁴, and Li Li^{1*}

¹Key Laboratory of Organic Compound Pollution Control Engineering (MOE), School of Environmental and Chemical Engineering, Shanghai University, Shanghai, 200444, China

²Office of Research and Development, U.S. Environmental Protection Agency, Research Triangle Park, North Carolina, USA

³Department of Earth and Atmospheric Sciences, University of Houston, Houston, USA

⁴Oak Ridge Institute for Science and Engineering (ORISE), Office of Research and Development, U.S. Environmental Protection Agency, Research Triangle Park, North Carolina, USA. Now at: SciGlob Instruments and Services, LLC., 9881 Broken Land Pkwy, Columbia, MD 21046, USA

Correspondence to: Li Li (lily@shu.edu.cn) and Yangjun Wang (yjwang326@shu.edu.cn)

Abstract

Chemical mechanisms are one of the major sources of bias in chemical transport model simulations, making their improvement a critical step towards enhancing model performance and supporting air quality management and research. In this study, a newly developed chemical mechanism, the Community Regional Atmospheric Chemistry Multiphase Mechanism (CRACMM), integrated into the Community Multiscale Air Quality (CMAQ) modeling system, was evaluated through comparison with two traditional chemical mechanisms, Carbon Bond 6 version r3 with aero7 treatment of SOA (CB6r3_ae7) and State Air Pollution Research Center version 07tc with extended isoprene chemistry and aero7i treatment of SOA (Saprc07tic_ae7i), for China. Sensitivity simulations related to precursor reactive organic carbon (ROC) emissions were conducted to investigate the key driving factors of PM_{2.5} formation. The results show slight differences in the correlation coefficient (R), mean bias (MB), and normalized mean bias (NMB) values for the three chemical mechanisms when using the traditional primary organic aerosol (POA) inventory. The results indicate that, when using the traditional primary organic aerosol (POA) inventory, the differences among the three chemical mechanisms are within 0 - 0.14 for the R, 0 - 10 µg/m³ for the MB, and within 10% for the NMB values. However, when using the full volatility emission inventory, CRACMM shows improvements in R, MB, and NMB values in some regions. However, when the full-volatility

设置了格式: 字体颜色: 文字 1

设置了格式: 字体颜色: 文字 1

设置了格式: 字体颜色: 文字 1

设置了格式: 字体颜色: 文字 1

带了格式: 正文

设置了格式: 字体: (默认) Times New Roman, 字体颜色: 文字 1

设置了格式: 字体颜色: 文字 1

设置了格式: 字体: (默认) Times New Roman, 字体颜色: 文字 1

设置了格式: 字体颜色: 文字 1

设置了格式: 字体: (默认) Times New Roman, 字体颜色: 文字 1

设置了格式: 字体颜色: 文字 1

设置了格式: 字体: (默认) Times New Roman, 字体颜色: 文字 1

设置了格式: 字体: Times New Roman, 字体颜色: 文字 1

34 emission inventory is applied in January, CRACMM exhibits improved performance in the
35 Pearl River Delta (PRD) region. The MB is reduced by 3.0-7.8 $\mu\text{g}/\text{m}^3$. In addition, the NMB
36 decreases by 17-23%, and the root mean square error (RMSE) is reduced by 1- 6 $\mu\text{g}/\text{m}^3$
37 compared with simulations using the traditional POA inventory across the four months.
38 CRACMM predicts higher $\text{PM}_{2.5}$, $\text{PM}_{2.5}$ concentrations during spring, summer and autumn,
39 mainly due to enhanced secondary organic aerosol (SOA) formation driven by increased
40 precursor emissions. Benzene-toluene-xylene (BTX) species and semi-volatile organic
41 compound (SVOC) emissions significantly contributed to $\text{PM}_{2.5}$ formation in CRACMM. The
42 SOA from BTX emissions accounts for nearly 50% of the $\text{PM}_{2.5}$ changes, while intermediate-
43 volatility organic compounds (IVOC) and SVOCs emissions mainly affect $\text{PM}_{2.5}$ concentrations
44 through SOA formation. These results indicate that CRACMM, when using the full-volatilefull-
45 volatility inventory, can effectively compensate for the underestimation of $\text{PM}_{2.5}$ mass that may
46 occur with traditional POA treatment, particularly in regions with high photochemical activity
47 and abundant S/IVOC precursors.

- 设置了格式: 字体颜色: 文字 1
- 设置了格式: 字体: Times New Roman, 字体颜色: 文字 1
- 设置了格式: 字体颜色: 文字 1
- 设置了格式: 字体: Times New Roman, 字体颜色: 文字 1
- 设置了格式: 字体: 11 磅, 字体颜色: 文字 1
- 设置了格式: 字体颜色: 文字 1

48 1. Introduction

49 Exposure to airborne $\text{PM}_{2.5}$ is associated with a variety of harmful health effects (Liu et al.,
50 2024; Tsai et al., 2025; Kim et al., 2015) and was reported to cause 4.14 million deaths
51 worldwide annually (95% confidence interval: 3.45 to 4.80) (Murray et al., 2020). underscoring
52 the highly need for effective mitigation of $\text{PM}_{2.5}$ pollution. Thus, a better understanding of the
53 $\text{PM}_{2.5}$ formation mechanism is essential for formulating effective air pollution control strategies.

- 设置了格式: 字体: 加粗, 字体颜色: 文字 1
- 设置了格式: 字体颜色: 文字 1

54 Chemical transport models such as the Community Multiscale Air Quality (CMAQ) model
55 (Byun and Schere, 2006) have been widely applied in China to investigate air quality issues,
56 including seasonal $\text{PM}_{2.5}$ and ozone distributions and their formation mechanisms. The CMAQ
57 version 5.02 and 5.3.2, both versions are equipped with the gas-phase mechanism of State Air
58 Pollution Research Center version99 (Saprc99) and Carbon Bond 6 version (CB6). These two
59 chemical mechanisms were employed to simulate air quality over China during 2013-2019
60 (Mao et al., 2022). In that study, $\text{PM}_{2.5}$ were examined in the North China Plain (NCP), Yangtze
61 River Delta (YRD), and Pearl River Delta (PRD), while it was overestimated in the Chengyu
62 Basin (CY) and Fen-Wei Plain (FWP) regions with NMB and NME values greatly exceeded

- 设置了格式: 字体: Times New Roman, 字体颜色: 文字 1
- 带格式的: 两端对齐, 段落间距段后: 0 磅, 行距: 1.5 倍行距
- 设置了格式: 字体: Times New Roman, 字体颜色: 文字 1
- 设置了格式: 字体: Times New Roman, 字体颜色: 文字 1
- 设置了格式: 字体: Times New Roman, 字体颜色: 文字 1
- 设置了格式: 字体: Times New Roman, 字体颜色: 文字 1
- 设置了格式: 字体: Times New Roman, 字体颜色: 文字 1
- 设置了格式: 字体: Times New Roman, 字体颜色: 文字 1

63 the suggested criteria. In addition, the FWP and CY also showed lower R than the benchmark
64 ($R < 0.4$) suggested by Emery et al during heavy polluted episode (Emery et al., 2017). During
65 2014–2017, the Comprehensive Air Quality Model with Extension (CAMx) (Yarwood et al.,
66 2007), version 6.2, version 7.1, CMAQv5.0.2, and CMAQv5.3.2 models performed quite well
67 in $PM_{2.5}$ mean performance. The bias and error terms of the four models were resemblant small:
68 -0.29 , -0.07 , -0.04 , and -0.11 for NMB and 0.51 , 0.48 , 0.53 , and 0.52 for NME, 0.58 , 0.55 ,
69 0.60 , and 0.39 , for R respectively (Meng et al., 2026). the CAMx6.2, CAMx7.1, and
70 CMAQv5.0.2 simulations covered the entire country, whereas CMAQv5.3.2 was evaluated
71 over eastern China. (Meng et al., 2026). According to Kang et al's research, the model shows
72 good performance for $PM_{2.5}$ in most areas, except for the PRD region, where the mean fractional
73 biases (MFB) for $PM_{2.5}$ using Saprc serious mechanisms are slightly outside the recommended
74 range (Boylan and Russell, 2006). According to Huang's research, evaluation results of $PM_{2.5}$
75 simulation by SOAP3 in CAMx in BTH, YRD, PRD, FWP, SCB and PRD areas, the R values
76 are 0.31 , 0.45 , 0.38 , 0.48 , and 0.15 in July, respectively. In November, the R values are also low
77 for PRD and FWP, 0.30 and 0.48 , respectively. (Huang et al., 2024).
78 Existing studies indicate that different chemical mechanisms vary significantly in terms of the
79 number of species, reaction complexity, and the coverage of chemical pathways, could lead to
80 noticeable differences in regional air quality model performance. With this realization, we
81 further examined the limitations of the commonly used chemical mechanisms (CB, Saprc and
82 Regional Atmospheric Chemical Mechanism (RACM)). In CB mechanism, model species
83 represent the concentrations of constituent groups regardless of the molecule to which they are
84 attached. Initially, this approach conserved carbon atoms, required relatively few species, and
85 both led to lower computational cost. However, as the mechanism evolved, its grouping
86 increasingly resembled aggregated molecule schemes, since both molecular structure and total
87 molecular weight significantly influence atmospheric chemistry (Yarwood et al., 2005). The
88 disadvantage of CB mechanism is that chemical expression of free radicals is insufficient (Kang
89 et al., 2016; Sarwar et al., 2008). Comparative analysis of different CB6 mechanism variants
90 shows that differences in reaction pathways can lead to significant deviations in model
91 predictions of ozone, NO_x , and formaldehyde (Cao et al., 2021).
92 The Saprc series (Saprc -90, Saprc -99, Saprc -07) aggregate VOCs by molecule or functional

设置了格式: 字体: Times New Roman, 字体颜色: 文字 1

设置了格式: 字体颜色: 文字 1

设置了格式: 字体: Times New Roman, 字体颜色: 文字 1

设置了格式: 字体: Times New Roman, 字体颜色: 文字 1

带格式的: 两端对齐, 缩进: 首行缩进: 0 字符, 段落间距段后: 0 磅, 行距: 1.5 倍行距

设置了格式: 字体: Times New Roman, 字体颜色: 文字 1

93 group, representing roughly 400 categories. Condensed versions are widely used in urban and
94 regional air quality models, but simplifications can limit the accuracy of organic chemistry
95 representation (Stockwell et al., 2012). Comparative analyses of different Sapr variants reveal
96 discrepancies in predicting ozone, radical species, and oxidative products, indicating
97 uncertainties arising from mechanism and emission inventories (Kang et al., 2025). For RACM,
98 it was developed for broader applications, where NO_x is lower and slower-reacting organics
99 are more important. RACM version 2 includes 118 species and 356 reactions. Even though this
100 mechanism is computationally efficient, however, it may inadequately capture detailed organic
101 chemistry and secondary organic aerosol (SOA) formation, resulting with potential
102 uncertainties in air quality predictions (Stockwell et al., 2012).
103 In air quality models, gas-phase chemical mechanisms are typically coupled with aerosol
104 modules to simulate interactions between the gas and particulate phases. Aerosol Module 7
105 (aero7) is the latest aerosol representation within the CMAQ model (Byun and Schere, 2006),
106 developed by the U.S. Environmental Protection Agency (EPA). Aero7 improves consistency
107 in representing SOA formation pathways between the CB- and SAPRC-based chemical
108 mechanisms. It also updates monoterpene SOA yields from photooxidation, adds uptake of
109 water onto hydrophilic organics, and includes consumption of inorganic sulfates (SO₄²⁻) when
110 isoprene epoxydiol (IEPOX) organosulfates are formed (Pye et al., 2013). Furthermore, it
111 enhances computational efficiency by using a volatility basis set (VBS) to parameterize SOA
112 yields rather than using the Odum 2-product fit (Zhang et al., 2021a).
113 Most of the above chemical mechanisms and SOA treatment exhibit substantial limitations in
114 simulating SOA formation (Wang et al., 2019; Zhang et al., 2021; Zhang et al., 2022; Zhang et
115 al., 2023; Huang et al., 2024). First, Semi-Volatile Organic Compounds (SVOC) and
116 Intermediate-Volatility Organic Compounds (IVOC) species are not explicitly represented,
117 leading to an underestimation of SOA contribution from those precursors. Even in 2D-VBS
118 mechanisms, which includes S/IVOC species, the gas-to-particle conversion of oxidative
119 products are mainly characterized using empirical parameters (e.g., yields and volatility
120 distributions). Moreover, the 2D-VBS framework does not explicitly track individual chemical
121 reactions; instead, it relies on parameterizations derived from environmental chamber
122 experiments or model calibration data, making it difficult to resolve specific chemical pathways

设置了格式: 字体: Times New Roman, 字体颜色: 文字 1

设置了格式: 字体: Times New Roman, 字体颜色: 文字 1

设置了格式: 字体颜色: 文字 1

设置了格式: 字体: Times New Roman, 字体颜色: 文字 1

带格式的: 两端对齐, 缩进: 首行缩进: 0 字符, 段落间距段后: 0 磅, 行距: 1.5 倍行距

设置了格式: 字体: Times New Roman, 字体颜色: 文字 1

设置了格式: 字体: Times New Roman, 字体颜色: 文字 1

123 of SOA formation (Chang et al., 2022). Second, the use of fixed-yield empirical
124 parameterization limits the representation of multigenerational oxidative processes and gas-
125 particle partitioning dynamics (Chang et al., 2022). Third, POA is commonly assumed to be
126 non-volatile and non-reactive, thereby neglecting its potential for re-evaporation and
127 subsequent oxidation to form SOA. These simplifications overly idealize SOA formation
128 processes missing various key reactions and resulted in an inaccurate representation of the
129 complex aging of organic aerosols in the atmosphere (Huang et al., 2024).
130 The Community Regional Atmospheric Chemistry Multiphase Mechanism (CRACMM) is the
131 latest chemical mechanism developed under the leadership of scientists at the US EPA.
132 CRACMM is built upon version 2 of RACM (Goliff et al., 2013) and incorporates state-of-the-
133 science developments, including autoxidation, aromatic chemistry, oxygenated hydrocarbons,
134 organic nitrates, and halogen chemistry. These advances enhance the representation of
135 atmospheric chemical transformations, enabling more realistic simulations of key air pollutants
136 such as O₃, PM_{2.5}, and various hazardous species, e.g. formaldehyde (Skipper et al., 2024). In
137 addition, CRACMM integrates a full-volatility organic framework and explicitly accounts for
138 multigenerational oxidative processes, thereby improving the physicochemical representation
139 of secondary organic aerosol (SOA) formation and providing a more comprehensive
140 description of SOA evolution (Ng et al., 2008).
141 CRACMM also provides detailed species mapping methodology between emission inventory
142 and chemical mechanism (Pye et al., 2023), to ensure carbon conservation when tracking the
143 transformation of carbon from emission sources to products (Ng et al., 2008). CB6r3 ae7 and
144 Saprc07tic ae7 do not consider certain SOA precursors such as L/S/IVOC (Chang et al., 2022),
145 and CRACMM explicitly accounts for SOA precursors beyond traditional non-oxygenated
146 volatile hydrocarbons, including phenolic compounds, furans, and other oxygenated organic
147 species (Pye et al., 2023). This makes CRACMM describing and simulating SOA in more
148 precise and accurate manner. No doubt CRACMM a good chemical mechanism candidate to
149 address the above listed shortcomings. CRACMMv1.0 was applied in the simulation over
150 northeast U.S. in summer reported in the work by Place et al (2023), and the result showed
151 ozone simulated values were better than RACM2 ae6 chemical mechanism in terms of
152 comparing with observation: average bias of RACM2 ae6 is +4.2ppb, average bias of

设置了格式: 字体: Times New Roman, 字体颜色: 文字 1

带格式的: 两端对齐, 段落间距段后: 0 磅, 行距: 1.5 倍行距

设置了格式: 字体: Times New Roman, 字体颜色: 文字 1

153 CRACMMv1.0 +2.1 ppb. A few studies have been conducted using CRACMM but they all
154 focused on US CONUS domain(Place et al., 2023). CRACMM has been not applied on China
155 domain so thorough evaluation is a must.

设置了格式: 字体: Times New Roman, 字体颜色: 文字 1

设置了格式: 字体: Times New Roman, 字体颜色: 文字 1

156 For computational cost considerations, the number of species and reactions directly affects
157 model runtime. Mechanisms with larger numbers of species and reactions, such as
158 Saprc07tic_ae7i, which contains the largest number of reactions and species among the standard
159 CMAQ mechanisms, is the most computational expensive mechanism compared to simpler
160 mechanisms like CB6r3_ae7. In contrast, CB has fewer reactions and species. The primary
161 difference between CB6r3_ae7 Saprc07tic_ae7i, and CRACMM lies in the chemistry module.
162 Our tests indicate that CRACMM requires approximately 30–40% more computational time
163 than CB6r3_ae7, but 20–30% less than Saprc.

164 With advances in high-performance computing, CRACMM could also be applied in a global
165 scale. Particularly, the Model for Prediction Across Scales (MPAS) global meteorological
166 model has recently been successfully coupled with CMAQ, demonstrating the application of
167 CRACMM in the global MPAS-CMAQ coupled model framework (Wong et al., 2024). Also,
168 CRACMM is not restricted to CMAQ. The design of CRACMM follows a modular framework
169 for gas-phase chemistry and SOA formation, which does not rely on model-specific
170 assumptions. Therefore, in principle, CRACMM could be implemented in other regional
171 models, although additional effort would be required to adapt emission mapping and aerosol-
172 chemistry coupling.

设置了格式: 字体颜色: 文字 1

设置了格式: 字体颜色: 文字 1

设置了格式: 字体颜色: 文字 1

设置了格式: 字体: (默认) Times New Roman, 字体颜色: 文字 1

设置了格式: 字体颜色: 文字 1

设置了格式: 字体: (默认) Times New Roman, 字体颜色: 文字 1

173 The Chemical Transport Models (CTMs) serve as valuable tools for identifying factors
174 contributing to PM_{2.5} formation. They can reproduce a series of physical and chemical processes
175 that atmospheric pollutants undergo after being emitted into the atmosphere, driven by emission
176 inventory data and meteorological fields. Gas phase chemical reaction mechanisms are an
177 essential part of the CTMs. Condensed mechanisms such as the Carbon Bond (CB) mechanism
178 (Yarwood et al., 2005; Yarwood et al., 2010) and the Statewide Air Pollution Research Center
179 (SAPRC) mechanism (Carter, 2010, 1999; Carter, 2000) are widely used in CTMs. In these
180 mechanisms, various volatile organic compounds (VOCs) are lumped into functional groups.
181 The CB chemical mechanism has evolved since the 1970s, with CB7 being one of the most
182 recent versions.

183 The SAPRC mechanism was first developed in the 1980s at the University of California,
184 Riverside. Saprc07 is one of the most widely used versions (Xie et al., 2013), which
185 introduces refinements for isoprene chemistry. It is commonly used in regulatory and research
186 applications requiring a detailed representation of VOCs. Saprc07 is a detailed, explicit
187 chemical mechanism that represents the atmospheric oxidation of a large number of VOCs,
188 providing a more nuanced representation of ozone formation and SOA production. Aero7 and
189 Aero7i modules contain the same major pathways to SOA, but AERO7i provides more
190 diagnostic information in terms of IEPOX SOA identification (Pye et al., 2017; Pye et al., 2013),
191 as well as some additional high NO_x formation pathways to SOA (Pye et al., 2015a).
192 CRACMM (Pye et al., 2023b) is a state-of-the-art atmospheric chemistry mechanism and was
193 introduced with the release of CMAQ version 5.4 in October 2022 by the U.S. EPA. CRACMM
194 integrates gas phase and particle phase reactions, offering a wide ranging representation of
195 atmospheric processes and enhanced capabilities for simulating multiphase chemistry in
196 regional air quality modeling. This approach helps models to more closely replicate
197 photochemical processes that occur in the atmosphere. CRACMM builds upon the well-
198 established Regional Atmospheric Chemistry Mechanism, version 2 (RACM2) framework
199 (Goliff et al., 2013) and incorporates enhanced representations of various organic compounds,
200 particularly monoterpenes and aromatics. Furthermore, CRACMM includes a built in,
201 transparent mapping of emissions to mechanism species, ensuring conservation of emitted
202 carbon while tracking its transformation in products. CB6r3_ae7 and Saprc07ie_ae7i typically
203 exclude organic species with saturation concentrations (C_i^*) in the low volatility organic
204 compound (LVOC, $0.3 < C_i^* < \mu\text{g m}^{-3}$), SVOC ($0.3 \leq C_i^* < 300 \mu\text{g m}^{-3}$) and IVOC ($300 \leq C_i^* <$
205 $3 \times 10^6 \mu\text{g m}^{-3}$) ranges, which act as potential precursors to SOA formation (Chang et al., 2022).
206 SOA precursors beyond traditional, non-oxygenated volatile hydrocarbons such as SVOCs,
207 phenolic compounds, furans, and other oxygenated organic compounds are considered in
208 CRACMM (Pye et al., 2023b).
209 Some previous studies have compared the model performance using various mechanisms in
210 CTMs. Luecken et al. (2019) compared CB6r3, CB5TU, and CB5 performances, and found
211 that CB6r3 performed best in simulating the vertical distribution of peroxyacyl nitrates.
212 Derwent et al. (2017) found that the condensed mechanisms (including CB6r3) and Master

213 ~~Chemical Mechanism version 3.3.1 (MCMv3.3.1) have large differences in predicted hydroxyl~~
214 ~~radical (HO₂) concentrations and their responses to NO_x and VOC reductions. For the SAPRC~~
215 ~~mechanism, Kang et al., (2022) evaluated a highly condensed SAPRC chemical mechanism~~
216 ~~and found that Saprc07 predicts slightly lower O₃ concentrations than the standard fix-~~
217 ~~parameter version of the Saprc11. CRACMM predictions were compared with RACM2 and~~
218 ~~CB6r3 over the northeastern US during summer. The results showed that CRACMM tends to~~
219 ~~predict more O₃ than CB6r3 but less than RACM2 (Place et al., 2023a). However, the PM_{2.5}~~
220 ~~predictions by the newly developed CRACMM mechanism and their sensitivities to precursors~~
221 ~~have not yet been investigated.~~

222 In this study, PM_{2.5} predictions from the CRACMM mechanism were evaluated with surface
223 observations comprehensively, covering different seasons and regions. Results derived by
224 CRACMM are compared with two well-established chemical mechanisms, Saprc07tic_ae7i
225 and CB6r3_ae7. The differences in PM_{2.5} and SOA drivers between CRACMM and the two
226 existing mechanisms are further explored. The results of this study provide a solid foundation
227 for the further application of CRACMM in understanding and regulating air pollution in China
228 and globally.

229 **2. Methodology**

230 **2.1 Model configuration**

231 Model simulations were conducted using CMAQ v5.4 with a horizontal resolution of 36 km ×
232 36 km, covering mainland China (Figure 1). This domain includes five key city clusters with
233 notable air pollution levels (Deng et al., 2022; Huang et al., 2024): Beijing-Tianjin-Hebei (BTH),
234 Yangtze River Delta (YRD), Pearl River Delta (PRD), Fen-Wei Plain (FWP), and Sichuan
235 Basin (SCB). Simulations were carried out for the months of January, April, July, and October
236 2021, representing winter, spring, summer, and autumn, respectively. The model includes 34
237 vertical layers, with the first layer located approximately 35 meters above the ground. Each
238 simulation was initialized with a 15-day spin-up period before the start of each month. In
239 addition to CRACMM version 1.0, two other chemical mechanisms, CB6r3_ae7 and
240 Saprc07tic_ae7i, were included for comparisons, the number of reactions and gas- and particle-
241 phase species in three different chemical mechanisms used in CMAQ are shown in Figure S1.

设置了格式: 字体颜色: 文字 1

设置了格式: 字体颜色: 文字 1

242 ~~Simple flowcharts illustrating the different species represented in each mechanism and their~~
243 ~~sources and sinks are shown in Figure S2 for CRACMM and Figure S3 for CB6r3_ae7. For~~
244 ~~Saprc07tic_ae7i, it has been described in detail in a previous studies (Pye et al., 2015b). All three~~
245 mechanisms are available in CMAQ-v5.4, with the "m3dry" deposition scheme selected. The
246 initial and boundary conditions for CRACMM and Saprc07tic_ae7i were mapped from the
247 seasonal average hemispheric CMAQ output files distributed through the CMAS_ Data
248 Warehouse. Meteorological input files were generated through an offline run of the Weather
249 Research and Forecasting (WRF) model (<https://www.mmm.ucar.edu/models/wrf>) version 4.0
250 with configurations detailed in our previous studies (Huang et al., 2021a). CMAQ ready
251 meteorological input files were created by the Meteorology-Chemistry Interface Processor
252 (MCIP) (Otte and Pleim, 2010) version 5.4 processing through output files from an offline run
253 of the Weather Research and Forecasting (WRF) model version 4.0 (Skamarock et al., 2019).
254 WRF configuration was detailed in our previous studies (Huang et al., 2021a). The archived
255 dataset, including the concentrations and model performance statistics of $PM_{2.5}$, $PM_{2.5-10}$ and its
256 components, model configurations, and the locations of all observation sites, is available on
257 Zenodo (Su and Chen, 2025) (Su et al., 2025).

设置了格式: 字体: Times New Roman, 字体颜色: 文字 1

设置了格式: 字体颜色: 文字 1

设置了格式: 字体颜色: 文字 1

设置了格式: 字体: Times New Roman, 字体颜色: 文字 1

设置了格式: 字体颜色: 文字 1

设置了格式: 字体: (默认) Times New Roman, 字体颜色: 文字 1

设置了格式: 字体颜色: 文字 1

设置了格式: 字体: (默认) Times New Roman, 字体颜色: 文字 1

设置了格式: 字体: (默认) Times New Roman, 字体颜色: 文字 1

设置了格式: 字体: (默认) Times New Roman, 字体颜色: 文字 1

设置了格式: 字体颜色: 文字 1

设置了格式: 字体: (默认) Times New Roman, 字体颜色: 文字 1

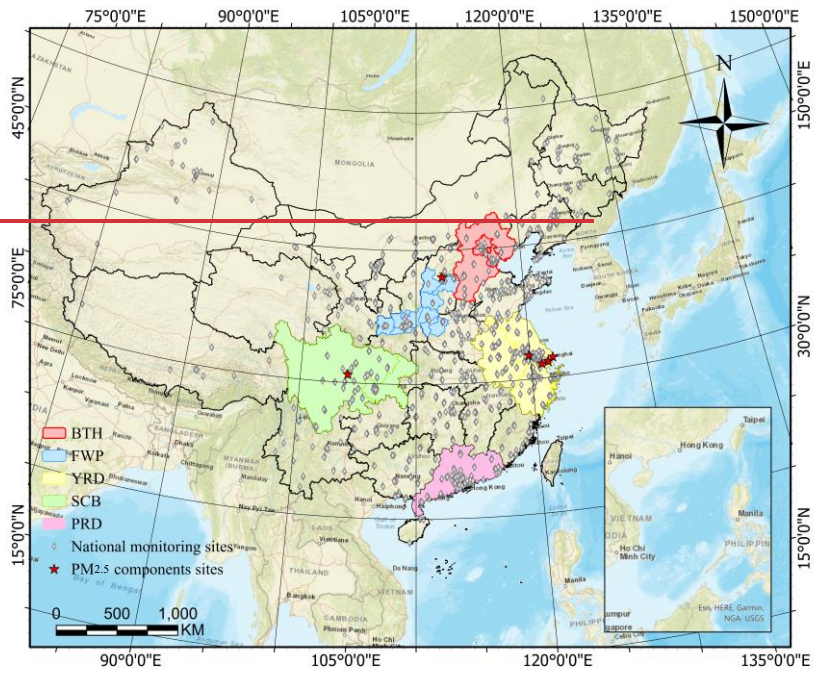
设置了格式: 字体颜色: 文字 1

设置了格式: 字体颜色: 文字 1

设置了格式: 字体: (默认) Times New Roman, 字体颜色: 文字 1

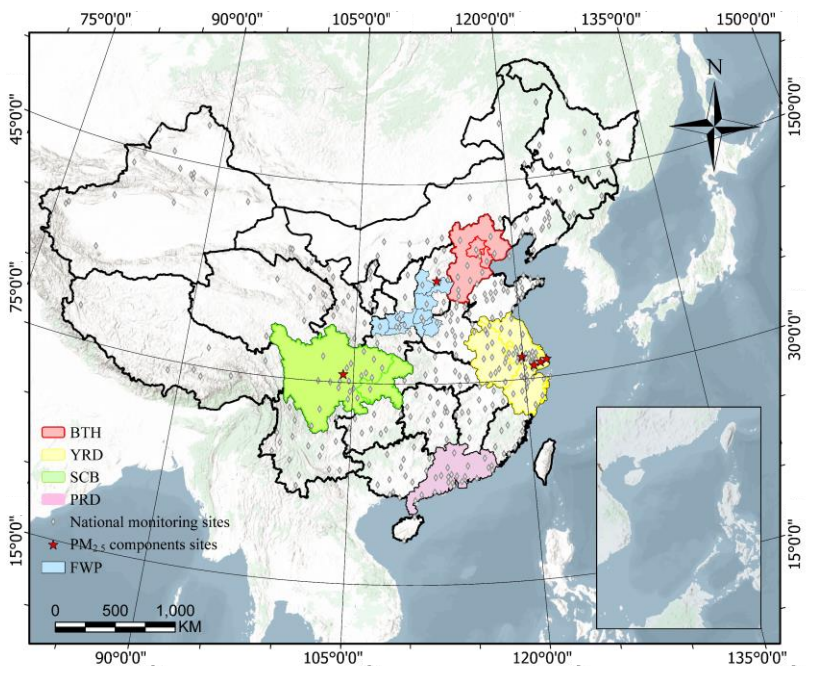
设置了格式: 字体: (默认) Times New Roman, 字体颜色: 文字 1

设置了格式: 字体颜色: 文字 1



设置了格式: 字体颜色: 文字 1
 设置了格式: 字体颜色: 文字 1

259



设置了格式: 字体颜色: 文字 1
 设置了格式: 字体颜色: 文字 1

260

261 **Figure 1.** Model domain with five **majorkey** city clusters (outlined in color), locations of
262 national monitoring sites (grey diamonds), and six PM_{2.5} chemical components observation
263 sites (red stars).

264 2.2 Emissions

265 2.2.1 Traditional Emissions Inventory

266 The 2019 anthropogenic Multi-resolution Emission Inventory for China (MEIC), developed by
267 Tsinghua University, was utilized in this study (<http://www.meicmodel.org>). Its spatial
268 resolution is 0.25° × 0.25° and includes five sectors: power, industry, residential,
269 transportation, and agriculture, and the provincial VOC emissions in 2019 from MEIC,
270 categorized by sector for January, April, July, October are shown in Tables S1-S4. Biogenic
271 emissions were estimated using the Model of Emissions of Gases and Aerosols from Nature
272 version 3.2 (MEGANv3.2, <https://bai.ess.uci.edu/megan/data-and-code/megan32>)
273 (Guenther et al., 2012). Currently, MEIC supports VOC emission only for both CB6r3_ae7 and
274 Saprc07tic_ae7i, but not the CRACMM mechanism. Therefore, anthropogenic VOC species
275 were converted to CRACMM input species using a binary decision tree approach. This
276 approach distinguishes between one-to-one and non-one-to-one mappings based on chemical
277 species correspondence from Saprc07tic_ae7i and CB6r3_ae7 to CRACMM. The one-to-one
278 mappings are further classified into explicit one-to-one (routine A) and lumped one-to-one
279 (routine B), while the non-one-to-one mappings include many-to-one (routine C) and many-to-
280 many (routine D) cases. In routine A, both Saprc07tic_ae7i and CB6r3_ae7 consist of a few
281 species that can be mapped directly to CRACMM based on CAS number, e.g., HCHO
282 (formaldehyde) is mapped to HCHO. In routine B, the mapping is based on lumped species
283 categories or names. For example, OLE1 (alkenes other than ethene, with $kOH < 7 \times 10^4 \text{ ppm}^{-1}$
284 min^{-1}) in Saprc07tic_ae7i is mapped to OLI (internal alkenes) in CRACMM, OLE2 (alkenes
285 with $kOH > 7 \times 10^4 \text{ ppm}^{-1} \text{ min}^{-1}$) is mapped to OLT (terminal alkenes), and ONIT is mapped to
286 RNO3 based on the same name used for organic nitrates.
287 In routine C, new species could be added to the CRACMM mechanism, such as CSL (Cresols)
288 and PHEN (Phenol and aromatic diols), which correspond to CRES (phenols and cresols) in
289 the Saprc07tic_ae7i mechanism. In this case, we use the emission factor ratio to distribute the
290 species. As MEIC does not provide species-level emission factors, data from the 2017 U.S.

带格式的: 行距: 1.5 倍行距

带格式的: 段落间距段后: 0 磅, 行距: 1.5 倍行距

设置了格式: 字体颜色: 文字 1

设置了格式: 字体颜色: 文字 1

设置了格式: 字体: (默认) Times New Roman, 字体颜色: 文字 1

设置了格式: 字体颜色: 文字 1

设置了格式: 字体: (默认) Times New Roman, 字体颜色: 文字 1

设置了格式: 字体: (默认) + 西文正文 (等线), (中文) + 中文正文 (等线), 字体颜色: 文字 1

设置了格式: 字体颜色: 文字 1

291 National Emission Inventory (NEI) (Pye et al., 2023b) were utilized, which contain over 3,000
292 species with corresponding emission factors, source sectors, and CRACMM species mappings.
293 The emission factors are averaged over all sources for different MEIC sectors (mobile sources,
294 industrial sources, etc.). Another example is that both XYE (P-xylene and less reactive
295 aromatics) and XYM (M-xylene and more reactive aromatics) are newly introduced species in
296 the CRACMM mechanism, corresponding to XYL (Xylene and other aromatics) in the
297 Saprc07tic_ae7i mechanism. According to the 2017 NEI, their ratio is 0.3:0.7. Therefore, 0.3
298 of XYL in Saprc07tic_ae7i is assigned to XYE in CRACMM, and 0.7 of XYL in
299 Saprc07tic_ae7i is assigned to XYM in CRACMM.

设置了格式: 字体颜色: 文字 1

设置了格式: 字体颜色: 文字 1

300 Routine D is more complicated, but the mapping is still based on the emission factor ratio for
301 proper mapping. For instance, in CRACMM, GLY represents both glyoxal and glycolaldehyde.
302 To construct this species from Saprc07tic_ae7i, GLY (representing glyoxal only) and part of
303 CCHO (glycolaldehyde and acetaldehyde) are mapped, such that GLY in CRACMM
304 corresponds to $GLY + CCHO \times 0.25$ in Saprc07tic_ae7i. Similarly, ACD (acetaldehyde) in
305 CRACMM corresponds to $CCHO \times 0.75$ in Saprc07tic_ae7i. For species lumped from multiple
306 species, only those with larger emission factors are considered. Table S4-S5 outlines the
307 correspondence relationships for major species with substantial emissions. Since it is
308 challenging to compare VOC emissions in different mechanisms due to the lumping rules, we
309 only conducted an overall comparison of total emissions, as shown in Table S2S6.

设置了格式: 字体颜色: 文字 1

设置了格式: 字体颜色: 文字 1

设置了格式: 字体颜色: 文字 1

设置了格式: 字体颜色: 文字 1

310 2.2.2 POA Emissions

311 Two POA inventories were employed in this study: a traditional POA emissions inventory and
312 a full-volatility inventory. CRACMM, Saprc07tic_ae7i, and CB6r3_ae7 all use the same
313 dataset for the traditional POA emissions inventory. This inventory applies a VBS profile based
314 on Woody et al. (2016) and Robinson et al. (2007), treating POA as semi-volatile with C_i^* values
315 ranging from 10^{-2} to $10^3 \mu\text{g}/\text{m}^3$. The detailed species of POA included in each mechanism are
316 listed in Table S3S7.

设置了格式: 字体颜色: 文字 1

317 In contrast, the full-volatility inventory distributes POA emissions across a wider range of
318 volatility bins. Laboratory experiments have demonstrated that L/S/IVOC emissions, which are
319 largely absent in the traditional POA inventory, contribute to SOA formation much more
320 efficiently than VOCs, owing to their lower volatility. To capture these processes, the full

带格式的: 两端对齐, 段落间距段后: 0 磅, 行距: 1.5 倍行距

设置了格式: 字体颜色: 文字 1

设置了格式: 字体颜色: 文字 1

351 of Low-Volatility Organic Compounds (LVOC) (1,342 kt/y), SVOC (1,169 kt/y), and IVOC
 352 (3,939 kt/y), resulting in a total of 6,450 kt/y. The new inventory fills a gap of 3,610 kt/y in
 353 L/S/IVOC emissions that were absent from the traditional inventory. To thoroughly evaluate
 354 CRACMM and compare it with CB6r3_ae7 and Saprc07tic_ae7i, four simulation scenarios
 355 were designed, as shown in Table 1.

356 In the CMAQ model, a potential combustion SOA (pcSOA) species is introduced to compensate
 357 for the fraction of SOA formed from the oxidation of combustion-related organic compounds
 358 that are not explicitly represented in the model (Murphy et al., 2017). Traditional chemical
 359 mechanisms often do not include SVOCs and IVOCs emitted from combustion sources, nor
 360 their associated oxidation pathways, which leads to a systematic underestimation of SOA levels
 361 in model simulations. To address this issue, CMAQ has incorporated the pcSOA species into
 362 the organic aerosol module since version 5.2, providing an empirical representation of this
 363 missing combustion-related SOA component (Murphy et al., 2017). This treatment is primarily
 364 intended for anthropogenic combustion sources, such as motor vehicle emissions, industrial
 365 combustion, and biomass burning. Because the CRACMM species framework explicitly
 366 accounts for multigenerational oxidation processes across different volatility ranges of VOCs,
 367 the empirical anthropogenic SOA source (pcSOA) implemented in the CB6r3_ae7 and
 368 Saprc07tic_ae7i mechanisms was turned off in all simulations to avoid double counting with
 369 the CRACMMv1.0 mechanism.

370 Additionally, the empirical representation of anthropogenic SOA source (pcSOA) (Murphy et
 371 al., 2017) was turned off in CB6r3_ae7 and Saprc07tic_ae7i, as pcSOA is deprecated in
 372 CRACMM.

373 **Table 1.** Description of simulation scenarios and their emissions

Scenarios	Mechanisms	POA emission inventory	Anthropogenic + Biogenic emission inventory
1	CB6r3_ae7	Traditional POA inventory	MEIC+MEGAN
2	Saprc07tic_ae7i	Traditional POA inventory	MEIC+MEGAN
3	CRACMM	Traditional POA inventory	MEIC+MEGAN
4	CRACMM	Full-volatile Full-volatility inventory	MEIC+MEGAN

374 **2.3 Observational data and model performance evaluation**

375 Hourly concentrations of PM_{2.5} at national monitoring stations were obtained from the China

设置了格式: 字体颜色: 文字 1
 设置了格式: 字体颜色: 文字 1

设置了格式: 字体颜色: 文字 1
 设置了格式: 字体颜色: 文字 1

设置了格式: 字体颜色: 文字 1
 带格式的: 段落间距段后: 0 磅, 行距: 单倍行距
 带格式的: 段落间距段后: 0 磅
 格式化表格
 设置了格式: 字体颜色: 文字 1
 带格式的: 段落间距段后: 0 磅
 设置了格式: 字体颜色: 文字 1

376 National Environmental Monitoring Centre (<http://air.cnemc.cn:18007>), which were then used
377 to evaluate model performance. Field observational data of PM_{2.5} chemical components
378 including NO₃⁻ (nitrate), SO₄²⁻, NH₄⁺ (ammonium), OC (organic carbon), and EC (elemental
379 carbon) at six super monitoring station sites were collected, as detailed in Figure 1 and Table
380 S4S9. Missing observation periods were excluded from the analysis. Model performance was
381 assessed using well-established statistical metrics, including the R, MB, NMB, root mean
382 square error (RMSE), normalized mean error (NME), and index of agreement (IOA). ~~The~~
383 ~~formulas for each individual parameter are presented in Table S10. In these equations, \bar{C}_m and~~
384 ~~\bar{C}_o represent the mean modeled and observed concentrations over all samples, respectively;~~
385 ~~$C_{m,i}$ and $C_{o,i}$ denote the modeled and observed values for the i -th sample; and N is the total~~
386 ~~number of valid samples. A combined analysis of these statistical indicators enables a~~
387 ~~comprehensive assessment of model performance and reliability, providing a basis for further~~
388 ~~model refinement and interpretation of the simulation results. The equations for calculating~~
389 ~~these metrics can be found in our previous study (Wang et al., 2024; Huang et al., 2021a).~~

391 3. Results and discussion

392 3.1 Overview of CMAQ-CRACMM model performance evaluation on PM_{2.5}

393 Figure 2 depicts the spatial distribution of observed (dots) and simulated PM_{2.5} concentrations
394 for January, April, July, and October 2021, based on the CRACMM model with the ~~full~~
395 ~~volatilefull-volatility~~ inventory. In January (Figure 2a), PM_{2.5} concentrations range from 5 to
396 over 100 µg/m³, with the highest values concentrated in the North China Plain (NCP) and parts
397 of the SCB. These elevated levels are primarily driven by relatively higher anthropogenic
398 emissions and stagnant meteorological conditions typical of winter. In April (Figure 2b),
399 concentrations have significantly decreased, ranging from 5 to 40 µg/m³, with the most notable
400 reductions observed in northern regions. During July (Figure 2c), PM_{2.5} concentrations were at
401 their lowest, typically ranging from 0 to 40 µg/m³. ~~This decline is mainly attributable to the~~
402 ~~increased precipitation and the associated washout of pollutants. In addition, higher planetary~~
403 ~~boundary layer (PBL) heights during the warm season, coupled with enhanced atmospheric~~
404 ~~mixing and dilution, further contributed to the decrease in PM_{2.5} concentrations. This decline is~~

设置了格式: 字体颜色: 文字 1

设置了格式: 字体颜色: 文字 1

设置了格式: 字体: (默认) Times New Roman, 字体颜色: 文字 1

设置了格式: 字体颜色: 文字 1

设置了格式: 字体: (默认) Times New Roman, 字体颜色: 文字 1

设置了格式: 字体颜色: 文字 1

设置了格式: 字体: (默认) Times New Roman, 字体颜色: 文字 1

设置了格式: 字体颜色: 文字 1

设置了格式: 字体: (默认) Times New Roman, 字体颜色: 文字 1

设置了格式: 字体颜色: 文字 1

设置了格式: 字体: (默认) Times New Roman, 字体颜色: 文字 1

设置了格式: 字体颜色: 文字 1

设置了格式: 字体: (默认) Times New Roman, 字体颜色: 文字 1

设置了格式: 字体颜色: 文字 1

设置了格式: 字体: (默认) Times New Roman, 字体颜色: 文字 1

设置了格式: 字体颜色: 文字 1

设置了格式: 字体: (默认) Times New Roman, 字体颜色: 文字 1

设置了格式: 字体颜色: 文字 1

设置了格式: 字体: (默认) Times New Roman, 字体颜色: 文字 1

设置了格式: 字体颜色: 文字 1

设置了格式: 字体: (默认) + 西文正文 (等线), (中文) + 中文正文 (等线), 字体颜色: 文字 1

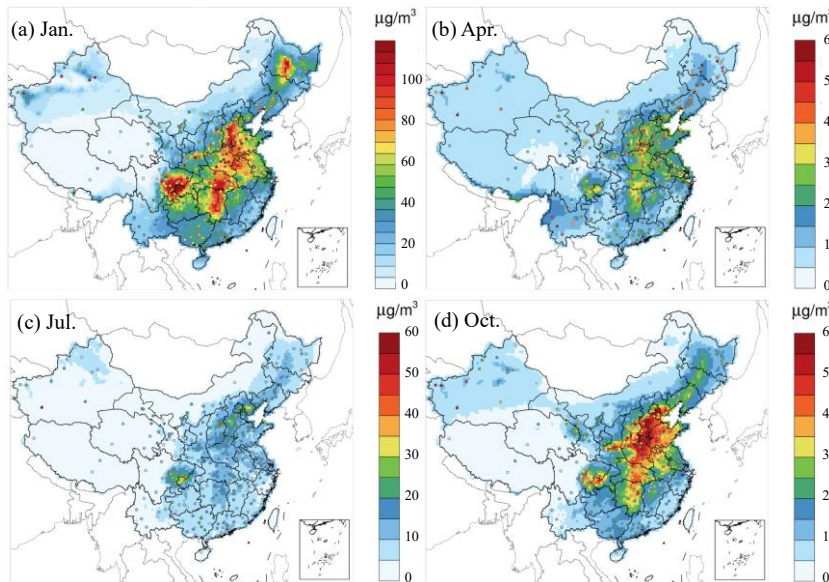
带格式的: 段落间距段后: 8 磅

设置了格式: 字体颜色: 文字 1

带格式的: 行距: 1.5 倍行距

设置了格式: 字体: Times New Roman, 字体颜色: 文字 1

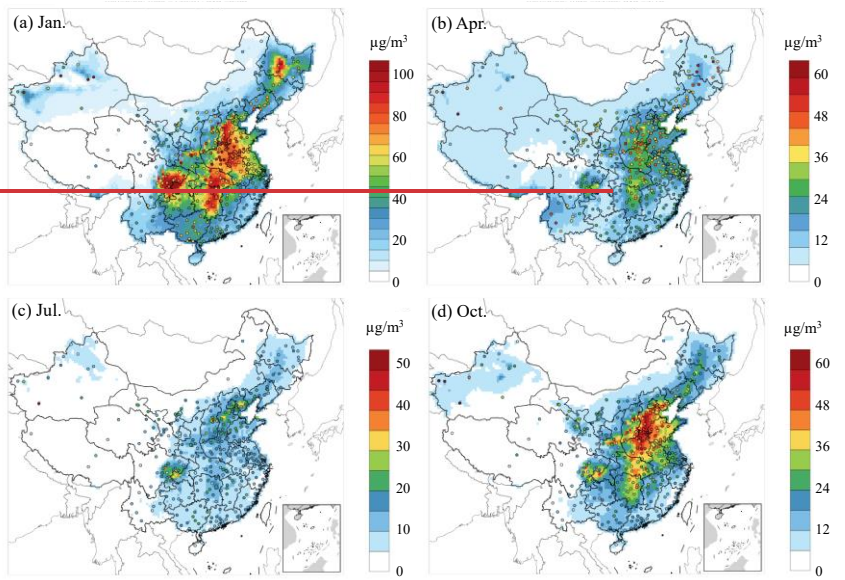
405 mainly attributable to the increased precipitation which washed out pollutants, in the southern
 406 and eastern parts of China compared to other months (Figure S5). In addition, higher planetary
 407 boundary layer (PBL) heights during the warm season in the south, particularly in the YRD
 408 region of China than other months (Figure S6), enhancing atmospheric mixing and dilution,
 409 and led to the decrease in PM_{2.5} concentrations. In October (Figure 2d), PM_{2.5} concentrations
 410 rise again, ranging from 5 to 60 $\mu\text{g}/\text{m}^3$, with the highest concentrations observed in the NCP
 411 and along the eastern coastal regions, which is attributed to the heating in later autumn and
 412 unfavorable meteorological conditions. Overall, monthly variations in PM_{2.5} concentrations are
 413 primarily driven by meteorological conditions and the distribution of emission sources.



- 设置了格式: 字体颜色: 文字 1
- 设置了格式: 字体: (默认) Times New Roman, 字体颜色: 文字 1
- 设置了格式: 字体颜色: 文字 1
- 设置了格式: 字体: Times New Roman, 字体颜色: 文字 1
- 设置了格式: 字体颜色: 文字 1
- 设置了格式: 字体: (默认) Times New Roman, 字体颜色: 文字 1
- 设置了格式: 字体: 11 磅, 字体颜色: 文字 1
- 设置了格式: 字体颜色: 文字 1

- 设置了格式: 字体颜色: 文字 1
- 设置了格式: 字体: (中文) + 中文正文 (等线), 小四, 字体颜色: 文字 1

414



415
 416 **Figure 2.** Monthly average PM_{2.5} concentrations predicted (raster) by CRACMM and observed
 417 (dots) in 2021 using the full-volatility emission inventory. Note that the color scale for panel
 418 (a) differs from panels (b-d) to highlight variations in the data.
 419 The performance of the CMAQ model in simulating hourly PM_{2.5} concentrations was evaluated
 420 by comparing the model outputs with observations from national monitoring sites. In January,
 421 CRACMM exhibited generally high R values in Northern China, indicating strong agreement
 422 between observed and simulated PM_{2.5} levels. In contrast, lower R values were observed in
 423 southern regions. The model demonstrated a negative bias across most areas (Figure 4a),
 424 suggesting a general underestimation of PM_{2.5} concentrations, except in the YRD and SCB
 425 regions, where positive biases are observed at many sites. This discrepancy is likely due, in part,
 426 to the frequent dust storm events in January of that year. Although both observations and model
 427 outputs from the major dust episodes on January 13–14 were excluded to minimize their
 428 influence on the monthly evaluation, the missing of dust emissions, the complex meteorological
 429 conditions associated with persistent northern dust layers may have contributed to an
 430 underestimation of PM_{2.5} concentrations by up to 30 µg/m³ in northern regions. Nevertheless,
 431 the model still achieves high R values in the BTH, YRD, and FWP regions. In January,
 432 CRACMM shows higher R value (R>0.7) over northern and eastern China (e.g., BTH, FWP).

设置了格式: 字体颜色: 文字 1

设置了格式: 字体: (默认) Times New Roman, 字体颜色: 文字 1

433 whereas lower R values (approximately 0.4) are found in southern regions (e.g., PRD)(Figure
434 3a). The model generally underestimates PM_{2.5} across most areas (Figure 4a), except for the
435 YRD and SCB regions, where positive biases occur at many sites. This spatial contrast is partly
436 attributable to dust-related influences, although data from the major dust episode on 13-14
437 January were excluded from the monthly evaluation, the absence of explicit dust emissions and
438 the associated complex meteorological conditions likely contributed to PM_{2.5} underestimation
439 of up to ~30 µg/m³ in northern China.

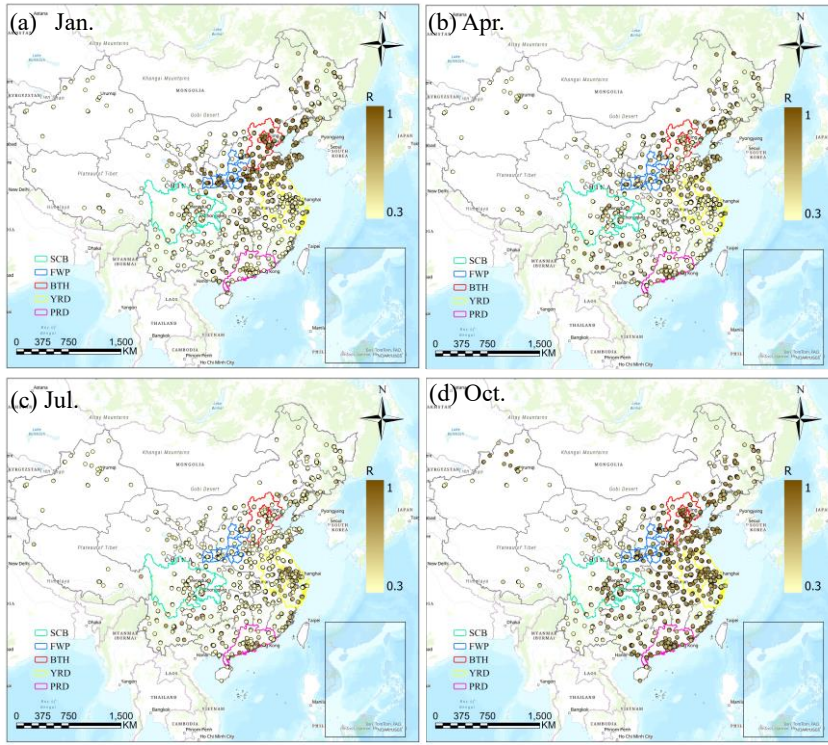
设置了格式: 字体颜色: 文字 1

设置了格式: 字体: Times New Roman, 字体颜色: 文字 1

440 Results for April (Figures 3b and 4b) show generally ~~good~~strong correlations in the eastern
441 regions, while several monitoring sites in the south exhibit lower R values. Compared to
442 January, the MB is less pronounced. April also experiences dust storm events. In July, R values
443 decline across all regions relative to January and April, and most stations exhibit relatively
444 small MB values (Figures 3c and 4c). The strong influence of temperature and solar radiation
445 on photochemical processes during summer may result in more pronounced diurnal variations
446 in chemical composition, making the simulation of chemical processes more challenging
447 (Seinfeld et al., 1998). Moreover, the chemical mechanisms may inadequately capture non-
448 linear interactions and the influence of SOA (Harrison et al., 2022), further reducing the
449 correlation. Additionally, synoptic-scale variations can also affect the spatial distribution and
450 concentration of key atmospheric species (Zhu et al., 2023). R values are improved in October
451 (Figures 3d and 4d), with 90% of the sites achieving R values of 0.8 and the MB is around 10
452 µg/m³ with higher evaluation in SCB and BTH regions. Overall, wintertime observed peaks
453 generally are underestimated and lower summertime observed values generally are well
454 captured. The model demonstrates strong performance in January and October, characterized
455 by higher correlations and smaller biases. However, it had weaker performance in April and
456 July with lower correlations.

设置了格式: 字体颜色: 文字 1

457



设置了格式: 字体颜色: 文字 1
 设置了格式: 字体颜色: 文字 1

458
 459 **Figure 3.** R values between predicted and observed $PM_{2.5}$ concentrations using CRACMM with
 460 the ~~full-volatile~~full-volatility emission inventory for January, April, July, and October of 2021.
 461 Figures S2-S7 and S83 compare the R and MB values between CRACMM (with ~~the full-~~
 462 ~~volatile~~the full-volatility inventory) and CB6r3_ae7 (with the traditional inventory). In January,
 463 CRACMM demonstrates notable improvements in R values at several sites in the PRD and
 464 YRD regions, with increases ranging from 0.2 to 0.4 (Figure S2a-S7a), while changes at most
 465 other sites remain relatively ~~minor~~minor (0-0.1). Regarding MB, the most pronounced
 466 differences also occur in January: some locations in the BTH and YRD regions show higher
 467 MB values—up to $10 \mu g/m^3$ —with CRACMM, whereas other ~~regions-sites~~ regions-sites display reduced
 468 MB values (Figure S3a-S8a). In April (Figures S2b-S7b and S3b-S8b), CRACMM achieves
 469 higher R values (0 - 0.2) at certain sites in the YRD, while slightly lower correlations (0-0.16)
 470 are observed in the PRD compared to CB6r3_ae7. MB values remain elevated in the SCB and
 471 parts of the YRD region for CRACMM. For July (Figures S2c-S7c and S3c-S8c), R values from
 472 CRACMM are generally comparable to those from CB6r3_ae7. However, MB values tend to

473 decrease across most regions, indicating a potential improvement in bias performance during
474 summer. In October, CRACMM shows moderate increases in R values—by approximately 0.1
475 at most sites (Figure S24S7d). MB values are lower in the PRD region but higher in the FWP
476 region compared to CB6r3_ae7 (Figure S24S8d).

477 In evaluating the CMAQ model's performance for hourly PM_{2.5} concentrations, CRACMM
478 generally shows good correlations with observed data in January and October. ~~However,~~
479 ~~discrepancies arise in April and July.~~ However, discrepancies arise in April, likely due to
480 chemical conditions such as dust storms, springtime dust events are frequently observed in
481 China, particularly in northern regions, driven by strong surface winds and synoptic-scale
482 transport (Huo et al., 2025). For July, larger discrepancies are likely associated with more
483 complex meteorological conditions, as reflected by the relatively poor performance of wind
484 speed, particularly in the SCB region. In contrast, the simulation performance of relative
485 humidity and temperature shows only minor differences relative to the other three months
486 (Tables S11–S13). In addition, photochemical activity typically peaks in the summer months
487 (June–August) due to stronger solar radiation and higher temperatures (Gu et al., 2022), which
488 further exacerbates these discrepancies.

489 –The model tends to underestimate peak PM_{2.5} concentrations during winter but captures lower
490 summer concentrations more accurately. Comparisons between CRACMM (with ~~the full-~~
491 ~~volatile~~the full-volatility inventory) and CB6r3_ae7 (using the traditional inventory) highlight
492 improvements in R values in the PRD and parts of the YRD regions in January for CRACMM,
493 although performance declines in July.

带格式的: 两端对齐, 段落间距段后: 0 磅, 行距: 1.5 倍行距

设置了格式: 字体颜色: 文字 1

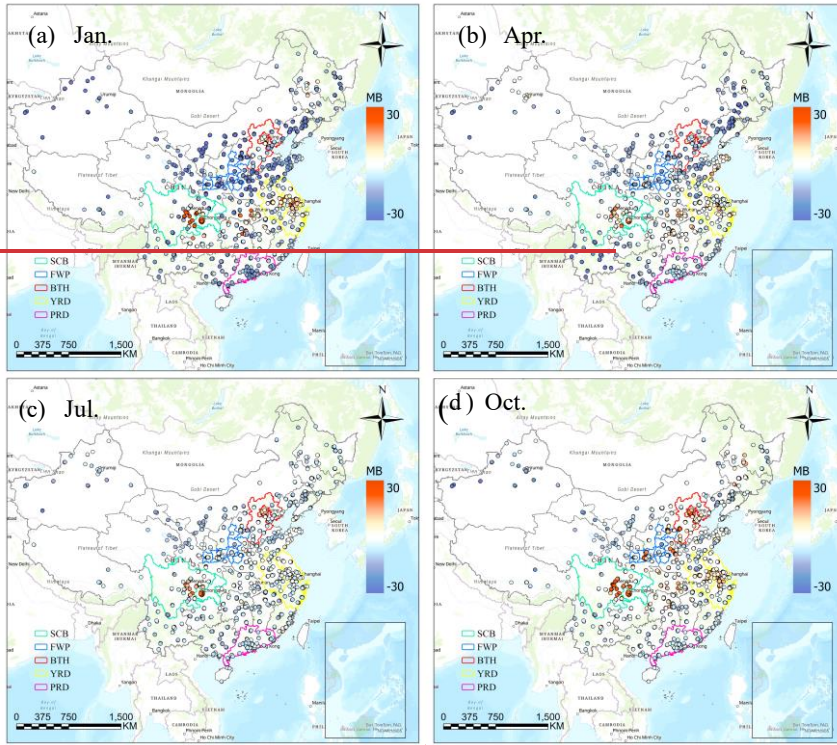
设置了格式: 字体颜色: 文字 1

设置了格式: 字体: Times New Roman, 字体颜色: 文字 1

设置了格式: 字体颜色: 文字 1

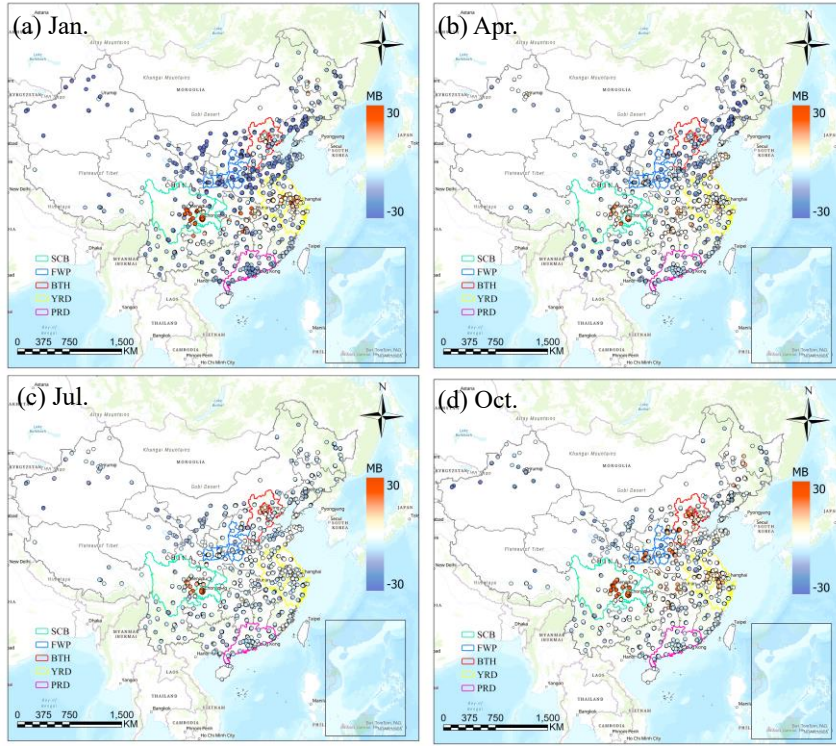
设置了格式: 字体颜色: 文字 1

设置了格式: 字体颜色: 文字 1



设置了格式: 字体颜色: 文字 1

设置了格式: 字体颜色: 文字 1



设置了格式: 字体颜色: 文字 1

设置了格式: 字体颜色: 文字 1

带格式的: 段落间距段后: 0 磅, 行距: 1.5 倍行距

设置了格式: 字体颜色: 文字 1

设置了格式: 字体颜色: 文字 1

设置了格式: 字体: Times New Roman, 字体颜色: 文字 1

设置了格式: 字体颜色: 文字 1

设置了格式: 字体: Times New Roman, 字体颜色: 文字 1

设置了格式: 字体颜色: 文字 1

设置了格式: 字体: Times New Roman, 字体颜色: 文字 1

设置了格式: 字体颜色: 文字 1

设置了格式: 字体: Times New Roman, 字体颜色: 文字 1

设置了格式: 字体颜色: 文字 1, 下标

设置了格式: 字体: Times New Roman, 字体颜色: 文字 1

设置了格式: 字体颜色: 文字 1

495

496 **Figure 4.** The MB values between predicted and observed PM_{2.5} concentrations using
 497 CRACMM with full-volatilefull-volatility inventory for January, April, July, and October of
 498 2021.

499 The simulation performance of PM_{2.5} components in six selected cities using CRACMM with
 500 the full-volatilefull-volatility inventory wasere evaluated. Some observations were from-The
 501 data of certain cities have been used their previous studies(Wang et al., 2024). Details for the
 502 selected cities are provided in Table S4, Tables S14-S17, summarize the statistical values of
 503 PM_{2.5} components, including NO₃⁻, SO₄²⁻, NH₄⁺, OC, and EC, for the four selected
 504 months. Tables S5-S8 present the statistical performance of PM_{2.5} components—including NO₃⁻,
 505 SO₄²⁻, NH₄⁺, OC, and EC—across four months. Figures S7S13-S16+0 demonstrate that
 506 CRACMM effectively captured the overall peaks and troughs of observed PM_{2.5} concentrations
 507 in January. The model also successfully simulated the heavy pollution period from January 20th
 508 to 25th in Taiyuan, with results similar to our previous study (Wang et al., 2024). The three ions
 509 were well simulated in both Changzhou and Pudong in the YRD region, particularly in

534 (Figure S4S9). The CRACMM simulation using the traditional inventory consistently results
535 in lower MB (Figure S5S10) and NMB (Figure S6S11) values compared to CB6r3_ae7 and
536 Saprc07tic_ae7i throughout the year, RMSE values range from for 0-2 $\mu\text{g}/\text{m}^3$ (Figure S12).
537 When the full-volatilefull-volatility inventory is incorporated, MB improves in April and July
538 but worsens in January and October. Similarly, NMB values indicate higher modeled
539 concentrations in all four months with the full-volatilefull-volatility inventory compared to the
540 traditional one. This trend is consistent with Figures S5, and 5, where the YRD region shows
541 higher modeled concentrations from CRACMM using the full-volatilefull-volatility inventory
542 than from both CB6r3_ae7 and Saprc07tic_ae7i across all months.

543 In the SCB region, R values remain relatively consistent across the three mechanisms (Figure
544 S4aS9a-c). A slight improvement is observed in July, where R increases from 0.22 with the
545 traditional inventory to 0.27 with the full-volatilefull-volatility inventory (Figure S4dS9d).
546 However, in October, R decreases from 0.62 to 0.56 after switching to the full-volatilefull-
547 volatility inventory. The increase in R value in July suggests that the traditional inventory may
548 underestimate key precursors (e.g., S/IVOCs), while the full-volatility inventory better captures
549 these species active at higher temperatures, improving model-observation agreement. In
550 contrast, the October decrease in R may reflect uncertainties in representing some gas- or
551 particle-phase organics under cooler conditions. Regarding MB, CRACMM generally shows
552 reduced values in most months when using the traditional inventory, except for April. With the
553 full-volatilefull-volatility inventory, MB decreases further in October, while slight increases are
554 observed in the other months. The trends in NMB follow a similar pattern to those in MB. It
555 could be due to overestimation of certain intermediate- or low-volatility species under specific
556 conditions.

557 In the PRD region, CRACMM exhibits notable performance improvements in January. As
558 shown in Figures S94a-c, the R value increases from 0.20 with CB6r3_ae7 and Saprc07tic_ae7i
559 to 0.35 when using CRACMM with the traditional POA inventory. When the full-volatilefull-
560 volatility inventory is applied (Figure S4dS9d), the R value further increases to 0.50.
561 Concurrently, the MB improves significantly, decreasing from $-19.6 \mu\text{g}/\text{m}^3$ to $-11.8 \mu\text{g}/\text{m}^3$, and
562 the NMB is reduced from -43% to -26% . These results indicate that CRACMM, particularly
563 with the full-volatilefull-volatility inventory, achieves both higher correlation and lower bias

设置了格式: 字体: Times New Roman, 字体颜色: 文字 1

设置了格式: 字体颜色: 文字 1

设置了格式: 字体: Times New Roman, 字体颜色: 文字 1

设置了格式: 字体颜色: 文字 1

564 for PM_{2.5} simulations in the PRD region during January. Under the traditional POA inventory,
565 CRACMM tends to underestimate PM_{2.5} concentrations in PRD during January (Figure
566 [S3aS8a](#)). However, after switching to the ~~full-volatile~~full-volatility inventory, simulated
567 concentrations exceed those predicted by CB6r3_ae7 (Figure 5a), primarily due to increased
568 contributions from SOA (Figure 8b). In comparison, during April and July, the CRACMM
569 simulations using the traditional emissions inventory showed lower R values than those of
570 CB6r3_ae7 and Saprc07tic_ae7i, and the correlation further declined when using the full-
571 volatility emissions inventory. Although CRACMM features a more comprehensive design for
572 gas-phase oxidation mechanisms, the intense photochemical activity in July and the rapid
573 oxidation of high concentrations of IVOC precursors may have introduced more complex SOA
574 formation pathways and product distributions, thereby increasing modeling uncertainties and
575 weakening the agreement with observations. By October, model performance had improved.
576 Across all months, CRACMM combined with the full-volatility emissions inventory
577 consistently outperformed the other mechanisms in terms of MB and NMB, highlighting the
578 critical role of this inventory in addressing the underestimation of ~~PM_{2.5}~~ PM_{2.5} associated with
579 traditional POA treatment.

580 In the FWP region, both the R (Figure [S4aS9a-c](#)) and MB (Figure [S5aS9a-c](#)) values show
581 minimal variation across the three mechanisms, indicating limited sensitivity to the chemical
582 mechanism alone. However, notable changes in MB and NMB are observed with the
583 incorporation of the ~~full-volatile~~full-volatility inventory in April, July and October, which align
584 with the higher PM_{2.5} concentrations shown in Figure 5, compared to CB6r3_ae7. In April and
585 July, MB values shift from -12.7 µg/m³ and -5.6 µg/m³ to -2.4 µg/m³ and 1.2 µg/m³, respectively,
586 with NMB showing a similar trend. These changes suggest an improvement in model agreement
587 when the ~~full-volatile~~full-volatility inventory is employed. In contrast, both MB and NMB
588 increase in October, indicating that the ~~full-volatile~~full-volatility inventory leads to higher
589 simulated concentrations during this month.

590 In the BTH region, The R (Figure [S4aS9a-c](#)) and MB (Figure [S5aS10a-c](#)) values remain largely
591 consistent across the three mechanisms. CRACMM with the traditional POA inventory shows
592 a decrease in R values from 0.44 to 0.38 compared to CB6r3_ae7 in July. After incorporating
593 the ~~full-volatile~~full-volatility inventory, the R in BTH experiences a more significant drop,

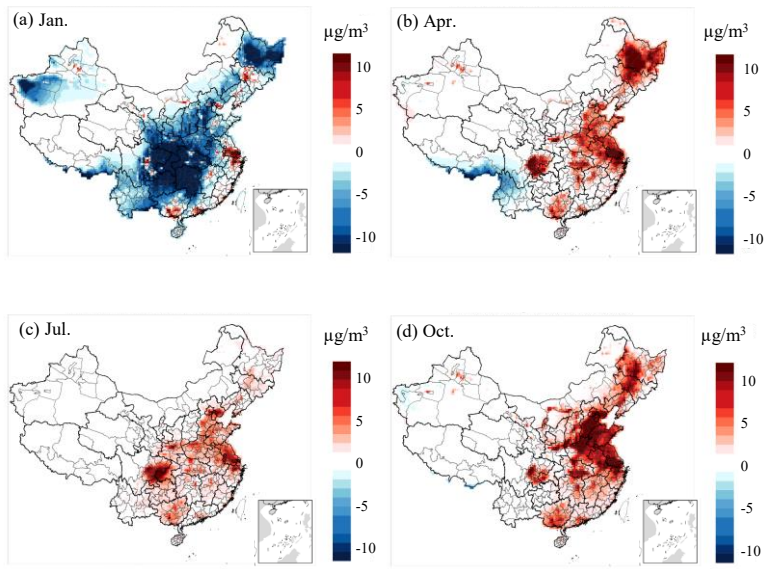
594 falling to 0.24. Notably, MB and NMB indicate that the modeled results are lower for
595 CRACMM with the traditional POA inventory in January, while they are higher in the other
596 months. Additionally, BTH exhibited the highest IVOC emissions in the inventory (Chang et
597 al., 2022), and uncertainties in emission estimates may have further contributed to this result.
598 Overall, the differences in R and MB values across the three chemical mechanisms are
599 relatively small when the traditional POA inventory is used. However, for CRACMM, the MB
600 in January indicates a stronger underestimation, primarily due to differences in POA (as shown
601 in Figure 8a), leading to lower modeled concentrations compared to CB6r3_ae7 and
602 Saprc07tic_ae7i. With the incorporation of the ~~full-volatile~~full-volatility inventory, the MB
603 shifts toward higher modeled concentrations in the subsequent three months. Notably, more
604 pronounced differences are observed in January in the PRD region and in July in the BTH
605 region.

606 3.2 Comparisons of model predicted PM_{2.5} between CRACMM and other mechanisms

607 Figures 5 and 6 illustrate the differences in model outputs between CRACMM with ~~full~~
608 ~~volatile~~full-volatility inventory and CB6r3_ae7, as well as between CRACMM and
609 Saprc07tic_ae7i. In January, CRACMM predicts lower PM_{2.5} concentrations across central and
610 northern China compared to both CB6r3_ae7 (Figure 5a) and Saprc07tic_ae7i (Figure 6a), with
611 the differences—up to 10 µg/m³—observed in central and north of China. While CRACMM
612 simulates higher ~~PM_{2.5}~~ PM_{2.5} concentrations in the PRD and YRD regions. For the remaining
613 months—April, July, and October—CRACMM with ~~full-volatile~~full-volatility inventory
614 generally predicts higher ~~PM_{2.5}~~ PM_{2.5} levels than the other two mechanisms (Figures 5b–d,
615 Figures 6b–d). When CRACMM and CB6r3_ae7 are configured with the traditional POA
616 inventory, as shown in Figure ~~S11~~S17, the differences of PM_{2.5} concentrations are reduced in
617 April, July, and October compared with ~~full-volatile~~full-volatility POA inventory. But
618 CRACMM still predicts lower ~~PM_{2.5}~~ PM_{2.5} levels than CB6r3_ae7 in January. A likely
619 explanation is that the lower photochemical activity leads to reduced SOA formation, as the
620 enhanced SOA pathways are less active during the winter months.

设置了格式: 字体颜色: 文字 1

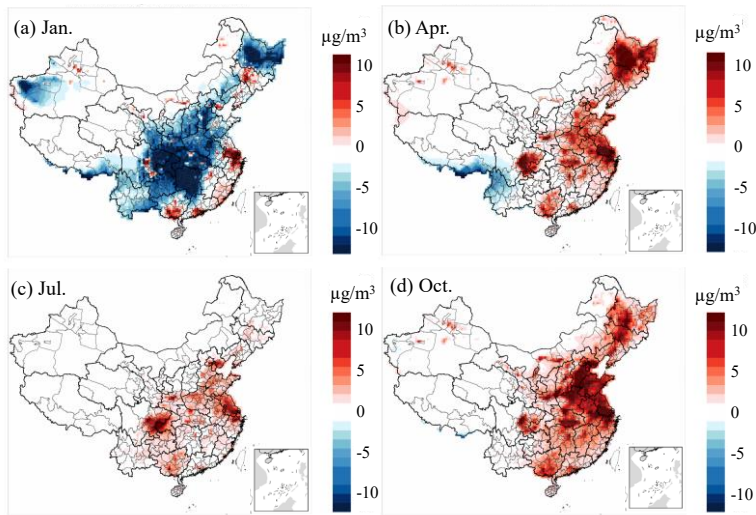
设置了格式: 字体颜色: 文字 1



设置了格式: 字体颜色: 文字 1
 设置了格式: 字体颜色: 文字 1

621

622 **Figure 5.** Differences in model-predicted PM_{2.5} concentrations between CRACMM (~~full~~
 623 ~~volatilefull-volatility~~ inventory) and CB6r3_ae7.



设置了格式: 字体颜色: 文字 1
 设置了格式: 字体颜色: 文字 1

624

625 **Figure 6.** Differences in model-predicted PM_{2.5} concentrations between CRACMM (~~full~~
 626 ~~volatilefull-volatility~~ inventory) and Saprc07tic_ae7i.

627 **3.3 Comparisons of model predicted PM_{2.5} chemical components between CRACMM**
628 **and other mechanisms**

629 Analysis of Figures 5, 6, and ~~S11~~S17 indicates that the most significant differences among the
630 model simulations occur in January and October, whereas the discrepancies between chemical
631 mechanisms are substantially smaller in April and July—likely due to the overall lower
632 pollutant concentrations during these months, which may reduce the sensitivity to mechanistic
633 differences. Consequently, the subsequent analysis focuses on a detailed comparison of PM_{2.5}
634 component variations between CRACMM and CB6r3_ae7 for January and October.

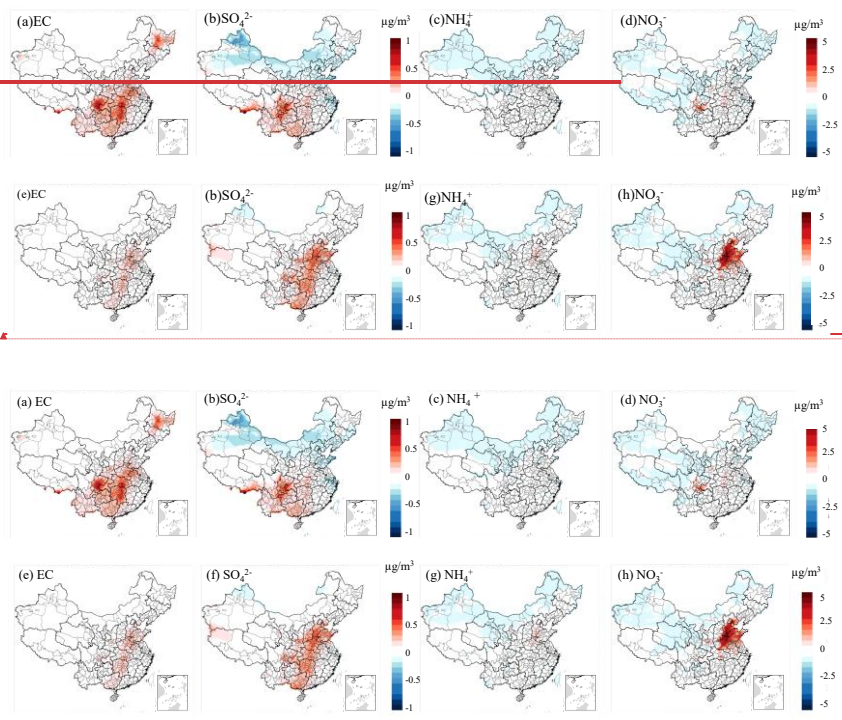
635 **3.3.1 Inorganic aerosol**

636 SO₄²⁻, NO₃⁻, and NH₄⁺ are the dominant secondary inorganic components in PM_{2.5}. Nitrogen
637 dioxide (NO₂) and sulfur dioxide (SO₂) can fully dissolve into cloud water or aerosol liquid
638 phases and subsequently oxidize to form nitrate and sulfate. Ammonium salts are produced
639 through the neutralization reactions of these acidic species with atmospheric ammonia (NH₃).
640 EC primarily originates from the incomplete combustion of carbonaceous fuels, especially
641 under oxygen-limited conditions. It is commonly emitted from sources such as vehicle exhaust,
642 industrial combustion, and biomass burning. From a chemical mechanism perspective,
643 CRACMM retains the inorganic chemistry framework of RACM2 but incorporates updated
644 rate constants for several reactions. Specifically, the rate expressions for 26 inorganic reactions
645 were revised in CRACMM compared to RACM2 (Pye et al., 2023b). Overall, differences in
646 inorganic component predictions among CRACMM, CB6r3_ae7, and Sapr07tic_ae7i are
647 relatively minor. As shown in Figure 7, predicted concentrations of major inorganic species in
648 January and October are comparable between CRACMM and CB6r3_ae7, with differences
649 ranging from -1 to 1 μg/m³ for EC and SO₄²⁻, and -5 to 5 μg/m³ for NH₄⁺ and NO₃⁻. These
650 results suggest that the variation in simulated inorganic aerosol concentrations is only
651 marginally affected by differences in the inorganic chemistry schemes.

设置了格式: 字体颜色: 文字 1

设置了格式: 字体颜色: 文字 1

设置了格式: 字体颜色: 文字 1



设置了格式: 字体颜色: 文字 1
 设置了格式: 字体颜色: 文字 1

设置了格式: 字体颜色: 文字 1
 设置了格式: 字体颜色: 文字 1

带格式的: 段落间距段后: 0 磅, 行距: 1.5 倍行距

设置了格式: 字体颜色: 文字 1

设置了格式: 字体颜色: 文字 1
 设置了格式: 字体: (默认) Times New Roman, 字体颜色: 文字 1

设置了格式: 字体颜色: 文字 1

652

653

654 **Figure 7.** Differences in model-predicted PM_{2.5} components—(a)EC, (b)SO₄²⁻, (c)NH₄⁺,
 655 (d)NO₃; for January, and (e)EC, (f)SO₄²⁻, (g)NH₄⁺, (h)NO₃; for October—between CRACMM
 656 (with full-volatilityfull-volatility inventory) and CB6r3_ae7. Figures (a–d) share the same scale,
 657 as do figures (e–h). Subplots (a–b) and (e–f) are plotted using the same color scale, as are
 658 subplots (c–d) and (g–h).

659 **3.3.2 Organic aerosol**

660 In January, CB6r3_ae7 consistently predicts higher POA concentrations than CRACMM under
 661 both the traditional and ~~full-volatility~~ volatile inventory configurations, with the most
 662 pronounced differences occurring in east China (Figure 8a and Figure S12aS18a). In
 663 CRACMM, POA aging is represented using a modified 2D-VBS framework (Murphy et al.,
 664 2017), where C_i^* range from 10⁻² to 10³ µg/m³. C_i^* represents the effective saturation
 665 concentration, which characterizes the volatility of organic compounds and influences gas-
 666 particle partitioning. A significant portion of the alkane-like L/SVOC mass contributing to

667 ambient OA comes from the direct emissions of low-volatility species (e.g., AROCN2ALK,
668 AROCN1ALK, AROCP0ALK, AROCP1ALK, AROCP2ALK, AROCP3ALK, where the
669 numbers indicate negative (N) or positive (P) $\log_{10}(C_i^*[\mu\text{g}/\text{m}^3])$ value. When species reside in
670 the gas-phase as a vapor, it is prefixed with a “V” and when in the particle phase, a prefix “A”
671 is used. For example, VROCP2ALK is an alkane-like vapor species with C_i^* of $10^2 \mu\text{g}/\text{m}^3$, and
672 AROCP2ALK is a particulate species of the same volatility.) and their oxidation products (e.g.,
673 AROCN2OXY2, AROCP0OXY2, AROCP1OXY1, AROCP2OXY2, AROCP3OXY2), these
674 species follow a similar naming convention as the L/S/IVOC alkanes, where numbers after N
675 and P indicate negative or positive $\log_{10}(C_i^*)$ value and the value ends in $10 \times nO:nC$ (e.g.,
676 ROCN2OXY2 is $C_i^* = 10^{-2} \mu\text{g}/\text{m}^3$ with $nO:nC=0.2$). By contrast, CB6r3_ae7 adopts a semi-
677 volatile POA approach in which primary emissions (e.g., LVPO1, SVPO1–3, IVPO1) and their
678 oxidation products (e.g., (LVOO1, LVOO2, SVOO1, SVOO2, SVOO3) partition between gas
679 and particle phases across a C_i^* range of 10^{-1} to $10^3 \mu\text{g}/\text{m}^3$. This framework aligns with the
680 1.5D-VBS scheme proposed by Koo et al. (2014). Details of the POA species and their
681 properties are provided in Table S3S7. The most significant differences in simulated POA
682 concentrations occur in January, likely due to enhanced partitioning of SVOC to the particle
683 phase under low wintertime temperatures. Additionally, differences in multigenerational
684 oxidation aging and volatility treatment between the two mechanisms contribute to the
685 simulation discrepancies. In October, although POA concentrations in CRACMM remain lower
686 than in CB6r3_ae7, the difference is less pronounced compared to January for both POA
687 inventory (Figures 8e and S12e).

688 To better understand the drivers of SOA formation in the two mechanisms, we analyzed the
689 spatial distribution of SOA concentrations under both traditional and full-volatile and full-
690 volatility POA inventories. In January, CRACMM predicts higher SOA levels in the BTH and
691 parts of the SCB regions compared to CB6r3_ae7 when using the traditional POA inventory
692 (Figure S12bS18b). Under the full-volatile the full-volatility inventory, CRACMM also shows
693 increased SOA concentrations in the YRD and PRD regions (Figure 8b). These increases
694 correspond with high IVOC emissions in BTH and YRD, consistent with the spatial patterns
695 reported by Chang et al. (2022), although their data reflect monthly averages across January
696 and July. The SOA enhancement in YRD and PRD under the full-volatile the full-volatility

设置了格式: 字体颜色: 文字 1, 下标
设置了格式: 字体颜色: 文字 1

设置了格式: 字体: Times New Roman, 字体颜色: 文字 1
设置了格式: 字体颜色: 文字 1
设置了格式: 字体: Times New Roman, 字体颜色: 文字 1
设置了格式: 字体颜色: 文字 1
设置了格式: 字体: Times New Roman, 字体颜色: 文字 1
设置了格式: 字体颜色: 文字 1
设置了格式: 字体: Times New Roman, 字体颜色: 文字 1
设置了格式: 字体颜色: 文字 1
设置了格式: 字体: Times New Roman, 字体颜色: 文字 1
设置了格式: 字体颜色: 文字 1
设置了格式: 字体: Times New Roman, 字体颜色: 文字 1
设置了格式: 字体颜色: 文字 1
设置了格式: 字体: Times New Roman, 字体颜色: 文字 1
设置了格式: 字体颜色: 文字 1
设置了格式: 字体: Times New Roman, 字体颜色: 文字 1
设置了格式: 字体颜色: 文字 1
设置了格式: 字体: Times New Roman, 字体颜色: 文字 1
设置了格式: 字体颜色: 文字 1
设置了格式: 字体: Times New Roman, 字体颜色: 文字 1
设置了格式: 字体颜色: 文字 1

设置了格式: 字体: (默认) + 西文正文 (等线), (中文) + 中文正文 (等线), 字体颜色: 文字 1
设置了格式: 字体颜色: 文字 1

设置了格式: 字体颜色: 文字 1
设置了格式: 字体颜色: 文字 1

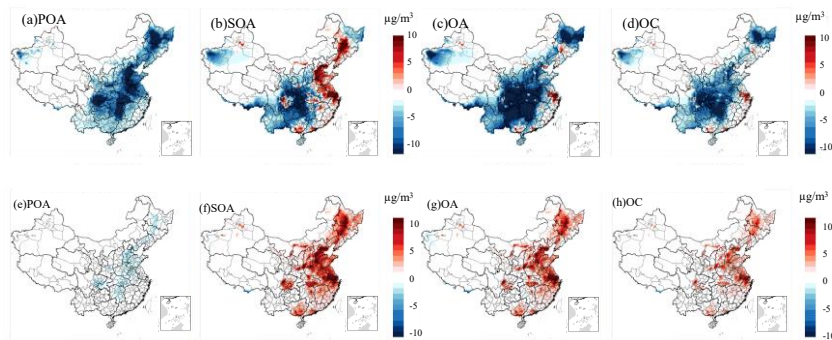
697 inventory highlights the critical role of IVOC emissions in these areas. In CB6r3_ae7, SOA is
698 primarily formed from the oxidation of traditional VOC sources, such as isoprene,
699 monoterpenes, sesquiterpenes, benzene, toluene, xylene, alkanes, and PAHs (Carlton et al.,
700 2010; Pye and Pouliot, 2012).

设置了格式: 字体颜色: 文字 1

设置了格式: 字体颜色: 文字 1

701 In contrast, CRACMM incorporates additional SOA precursor systems, including phenol and
702 aromatic diols, pinon aldehyde, oxygenated IVOCs, furanone, and other compounds. As a result,
703 in regions with elevated anthropogenic emissions, CRACMM generally simulates higher SOA
704 concentrations. However, in the SCB region, SOA levels remain lower, possibly due to the
705 reduced reactivity of these new precursors under the lower ambient temperatures typical of this
706 region. In terms of overall OA concentrations, CRACMM generally predicts lower values than
707 CB6r3_ae7 across most regions, except for some part of YRD region (Figure 8c and Figure
708 [S12eS18c](#)). The spatial distribution of OC is similar to that of OA, with CRACMM also
709 showing lower concentrations than CB6r3_ae7 (Figure 8d and Figure [S12dS18d](#)).

710 In October (Figures 8f-h and [S12fS18e-h](#)), SOA remains the dominant contributor to the
711 differences in PM_{2.5} concentrations. Under ~~the full-volatile~~[the full-volatility](#) inventory,
712 CRACMM predicts significantly higher SOA concentrations compared to CB6r3_ae7 (Figure
713 8f), resulting in elevated OA levels (Figure 8g). The spatial pattern of OC concentrations
714 (Figure 8h) closely resembles that of OA. When the traditional POA inventory is applied, the
715 differences in SOA, OC, and OA concentrations between the two mechanisms are minimal
716 (Figures [S12fS18e-h](#)). The most pronounced increases with ~~the full-volatile~~[the full-volatility](#)
717 inventory are observed in the YRD, PRD, and SCB regions, attributable to the inclusion of a
718 more comprehensive set of SOA precursors.



设置了格式: 字体颜色: 文字 1

设置了格式: 字体颜色: 文字 1

719 **Figure 8.** Differences in model-predicted PM_{2.5} components—(a) POA, (b) SOA, (c) OA, and
 720 (d) OC for January, and (e) POA, (f) SOA, (g) OA, and (h) OC for October—between
 721 CRACMM (with full-volatilefull-volatility inventory) and CB6r3_ae7. *Figures (a–d) share the*
 722 *same scale, as do figures (e–h).*

724 Overall, in January, the primary differences between CRACMM and CB6r3_ae7 stem from
 725 lower POA concentrations in CRACMM, primarily due to semi-volatile partitioning and
 726 reduced aging of semi-volatile POA species at lower temperatures. SOA concentrations are
 727 elevated in eastern China but reduced over the SCB, reflecting both the slower oxidation of
 728 additional SOA precursors under winter conditions in the SCB and the greater availability of
 729 these precursors in the eastern region. In October, the key differences in model predictions are
 730 primarily driven by the POA inventory used. The full-volatility inventory yields higher SOA
 731 concentrations than the traditional inventory, largely due to the inclusion of L/S/IVOCs, which
 732 are efficient SOA precursors.

733 3.4 Sensitivity study on PM_{2.5} and SOA responses to changes of precursors

734 In this section, CMAQ simulations with emission perturbations are conducted to identify the
 735 key drivers of PM_{2.5} formation in January, when PM_{2.5} concentrations are notably high. A series
 736 of emission sensitivity simulations were performed within CMAQ to assess the role of
 737 precursor ROC systems in PM_{2.5} formation using CRACMM with the full-volatilefull-volatility
 738 inventory across China. These sensitivity simulations involved running zeroed emission
 739 scenarios for January (i.e., setting emissions of a specific chemical class or sector to zero) to
 740 examine how PM_{2.5} concentrations respond to changes in emissions. A subset of these

741 sensitivity simulations was also conducted using the CB6r3_ae7 and Saprc07tic_ae7i
742 mechanisms. A detailed list of all the zeroed emission simulations is provided in Tables 3 and
743 S13S22. Due to the non-linear nature of PM_{2.5} production in response to ROC perturbations,
744 these simulations offer an initial evaluation of how PM_{2.5} formation responds to reduced ROC
745 emissions, providing valuable insights into how chemical systems behave under varying
746 emission conditions in the three mechanisms.

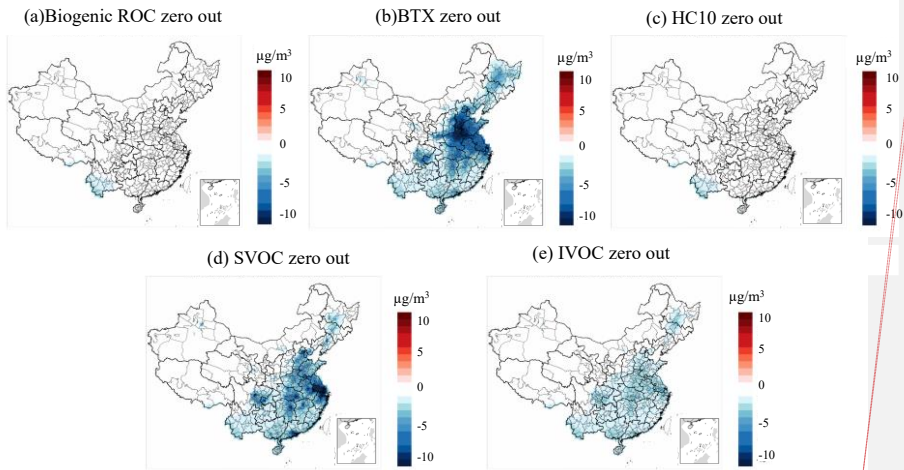
747 **Table 3.** List of emission reductions relative to the base simulations in CMAQ-CRACMM.

Chemical Mechanism	Emission Reduction
▲ CRACMM	Benzene, toluene and xylene-like emissions set to zero
▲ CRACMM	Biogenic-ROC emissions set to zero
▲ CRACMM	IVOC emissions set to zero
▲ CRACMM	SVOC emissions set to zero
▲ CRACMM	HC10 zero out (decane and species of similar reactivity)

748 Figure 9 shows domain-wide differences in average PM_{2.5} concentrations between the base
749 CRACMM simulation and a series of zeroed emission simulations. A similar spatial pattern in
750 PM_{2.5} response was observed for zeroed biogenic and HC10 emissions (Figures S13aS19a, c in
751 percentage and Figures 9a, c in concentration), with CRACMM predicting a modest 1% change
752 in PM_{2.5} and less than 3 μg/m³ in many parts of China. This can be attributed to the low SOA
753 yield by mass (0.09 g/g) for HC10 compounds (Pye et al., 2023), and the generally low winter
754 emissions of biogenic ROC, as shown in previous studies (Pye et al., 2023). Zeroing BTX
755 emissions resulted in average PM_{2.5} concentration changes of -20% to 0% (Figure S13bS19b)
756 and -10 to 0 μg/m³ (Figure 9b), particularly in the YRD and BTH regions, where BTX emissions
757 are highest. The high PM_{2.5} formation potential of BTX compounds is attributed to their overall
758 emission abundance and high SOA yield by mass (~0.5 g/g). Moreover, ozone levels in urban
759 areas with significant BTX emissions also decrease in the BTX zero-out scenario (Figure
760 S14S20). This effect is particularly evident in the PRD region, where the reduction reaches up
761 to 10 μg/m³. This aligns with the findings of Place et al. (2023). One factor is the removal of
762 BTX emissions, which serve as precursors for SOA formation. The second factor is that zeroing
763 BTX emissions leads to a decrease in O₃, which weakens atmospheric oxidizing capacity and
764 reduces SOA formation. However, it is important to note that Place's study was conducted in
765 summer.

带格式的: 行距: 单倍行距

设置了格式: 字体颜色: 文字 1

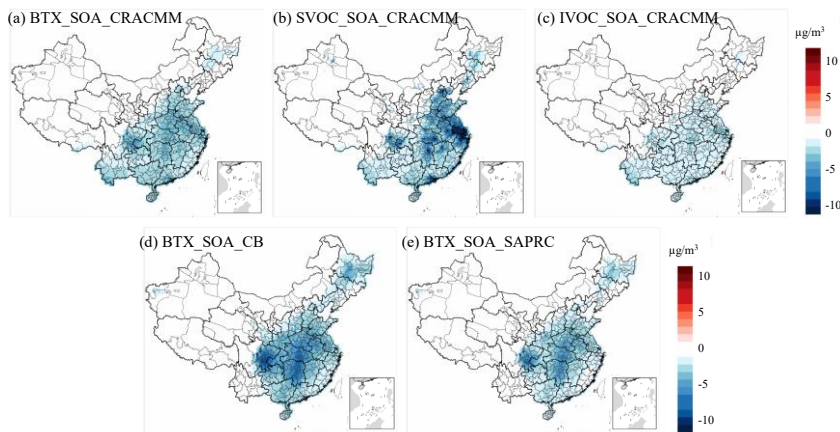


设置了格式: 字体颜色: 文字 1

设置了格式: 字体颜色: 文字 1

766

767 **Figure 9.** Changes in $PM_{2.5}$ concentrations between each zero-out scenario and its
 768 corresponding base simulation: (a) biogenic ROC emission, (b) BTX emission, (c) HC10
 769 emission, (d) SVOC emission, and (e) IVOC emission with CRACMM.



设置了格式: 字体颜色: 文字 1

设置了格式: 字体颜色: 文字 1

770

771 **Figure 10.** Changes in SOA concentrations between each zero-out scenario and its
 772 corresponding base simulation: (a) BTX emissions, (b) SVOC emissions, (c) IVOC emissions
 773 with CRACMM, (d) BTX emissions with CB6r3_ae7, (e) zeroed BTX emissions with
 774 Sapr07tic_ae6.

775 As shown in Figures 10a, d, and e, the impact of zeroing BTX species on SOA formation for
 776 the three mechanisms accounts for only approximately 50% of the total $PM_{2.5}$ change observed
 777 in Figures 9b, S16a and c. This suggests that the changes in $PM_{2.5}$ concentrations resulting from

778 the removal of BTX emissions are not solely due to SOA formation but may also involve other
779 pathways or chemical processes. In contrast, the influence of S/IVOC species on ~~PM_{2.5}~~
780 concentrations in the CRACMM mechanism is primarily driven by SOA formation. This
781 conclusion is supported by the spatial distribution and concentration differences shown in
782 Figures 9d, e, and Figures 10b, c, which exhibit nearly identical patterns. These similarities
783 indicate that the effects of S/IVOC emissions on PM_{2.5} are mainly driven by SOA production.
784 The largest PM_{2.5} response was observed when emissions from SVOC sources were excluded
785 from the simulation (Figure ~~S13d~~[S19d](#)), primarily because SVOCs have the highest yield,
786 exceeding 1.0 g/g. The percentage changes in PM_{2.5} range from -40% to 0%, with a
787 concentration reduction of more than -10 µg/m³ (Figure 9d), particularly in the YRD region,
788 where SVOC emissions are substantial. For IVOCs, the reduction is about -5% across much of
789 China, except in the western regions where IVOC emissions are very low (Figure ~~S13e~~[S19e](#)),
790 resulting in a reduction of less than -5 µg/m³ (Figure 9e).

791 A similar Δ ~~PM_{2.5}~~ response in percentage (Figure ~~S15~~[S21](#)) and concentration change
792 (Figure ~~S16~~[S22](#)) was observed when biogenic and BTX emissions were zeroed in simulations
793 using CB6r3_ae7_ae7 and Saprc07tic_ae7i. However, the CRACMM simulation with zeroed
794 biogenic emissions (Figure 9a) showed a more pronounced and widespread decrease in PM_{2.5}
795 compared to both CB6r3_ae7_ae7 and Saprc07tic_ae7i. This difference can be attributed to the
796 inclusion of new S/IVOC species in MEGAN, which are not accounted for in the other two
797 mechanisms. Additionally, zeroing BTX emissions had a greater impact in CB6r3_ae7,
798 particularly in central China, compared to Saprc07tic_ae7i and CRACMM. A possible reason
799 for this is that CRACMM reduces the number of lumped species in BTX and enhances the
800 representation of aromatic IVOC species, such as single-ring aromatics $\log_{10}(Ci^*) \approx 5$
801 (ROCP5ARO) and $\log_{10}(Ci^*) \approx 6$ (ROCP6ARO). These species are included in CB6r3_ae7
802 under categories like m-xylene and other more reactive aromatics (XYM), as well as less
803 reactive aromatics (XYE). As a result, CRACMM incorporates fewer species in BTX emissions
804 compared to CB6r3_ae7.

805 **3.5 Uncertainty Analysis and limitations**

806 **3.5.1 Limitations of VOC Speciation Mapping**

807 In the speciation mapping process, explicit species were directly mapped across the CRACMM,

808 CB6r3_ae7, and Saprc07tic_ae7i mechanisms, as these species are explicitly represented and
809 therefore allow for one-to-one mapping. Consequently, their spatial distributions were assumed
810 to be identical across the three mechanisms, and uncertainties associated with their emission
811 estimates were considered negligible. In contrast, lumped species present greater complexity
812 due to differences in the VOC species included within each lumped mechanism species. Given
813 that a direct one-to-one mapping between lumped species is not feasible, the mapping was
814 performed by matching the dominant lumped VOC species across mechanisms based on their
815 relative emission magnitudes. Overall, CRACMM incorporates a more comprehensive set of
816 VOC species than either CB6r3_ae7 or Saprc07tic_ae7i. The total mapped emissions associated
817 with each mechanism-specific inventory are summarized in Table S2S6. Nevertheless,
818 uncertainties remain due to regional differences in emission profiles. In particular, the total
819 emissions and source sector distributions of VOC species in Chinese emission inventories may
820 differ from those represented in the NEI. Such discrepancies introduce additional uncertainty
821 into the speciation mapping process.

822 3.5.2 Uncertainty in Mapping L/S/IVOC Emissions

823 ~~For L/S/IVOCs, the 2D-VBS framework was applied to aggregate predicted products into a~~
824 ~~reduced set of 15 representative CRACMM mechanism species. These representative species~~
825 ~~span a wide range of saturation concentrations (C_i^*) from 10^{-2} to 10^6 $\mu\text{g m}^{-3}$ and O:C ratios ($n\text{O}:$~~
826 ~~$n\text{C}$) from 0.1 to 0.8. The original 2D-VBS inventory is structured along a two-dimensional grid~~
827 ~~defined by $\log_{10}(C_i^*)$ and O:C ratio. During the mapping process to CRACMM, if a species in~~
828 ~~the 2D-VBS inventory could not be directly assigned to a CRACMM species, it was reassigned~~
829 ~~to the most proximate species in $\log_{10}(C_i^*)$ and/or O:C ratio. This reassignment process, while~~
830 ~~necessary, inevitably introduces additional uncertainty. The L/S/IVOC emission inventory used~~
831 ~~in this study is based on the work of Chang et al. (Chang et al., 2022). For uncertainties~~
832 ~~associated with this inventory, readers are referred to the analysis by Chang et al., which~~
833 ~~discusses uncertainties related to emission factors, species classification, and spatial~~
834 ~~distribution. For the species which can be mapped on a one-to-one basis in Table S8, the~~
835 ~~associated uncertainty is assumed to be zero. For species mapping involving the same $\log_{10}(C_i^*)$~~
836 ~~values, such as VROCP1OXY1, VROCP0OXY4, and VROCN2OXY4, some uncertainty may~~
837 ~~be introduced due to the proximity in volatility space. Anthropogenic L/S/IVOCs emission~~

设置了格式: 字体: 非加粗, 字体颜色: 文字 1

设置了格式: 字体: Times New Roman, 字体颜色: 文字 1

设置了格式: 字体: (默认) Times New Roman, (中文) + 中文正文 (等线), 11 磅, 字体颜色: 文字 1, 连字: 标准 + 上下文

设置了格式: 字体: (默认) Times New Roman, (中文) + 中文正文 (等线), 11 磅, 字体颜色: 文字 1, 连字: 标准 + 上下文

838 inventories for China (Figure S4) contains (a) particle-phase emissions with full-volatility
839 coverage and (b) gas-phase emission inventories (Chang et al., 2022). Based on uncertainties
840 of activity data and emission factors for each sector, the uncertainty of OA emissions can be
841 quantified using a Monte Carlo method. According to Chang et al.(2022), the overall
842 uncertainties at the 95% confidence interval for LVOC, SVOC, IVOC and VOC are (-40%,
843 +43%), (-35%, 38%), (-33%, +33%) and (-21%, +28%), respectively. The overall uncertainty
844 for L/S/IVOC is (-25%, +30%). Uncertainties across sectors tend to partially offset each other,
845 resulting in a total emission uncertainty that is often smaller than that of the individual sectors.
846 S/IVOC emissions from domestic Volatile Chemical Products (VCPs) have the largest
847 uncertainties (-81%, +143%), followed by open biomass burning (-58%, +81%) and industrial
848 VCPs (-50%, +65%). Although the emission factors are based on local experiments, emissions
849 from domestic fossil fuel and biomass burning still have considerable uncertainties (-38%,
850 +62%) and (-38%, +51%), respectively.

851 ▲ 852 **4. Conclusions**

853 This study introduces the newly mapped VOC and POA inventories (both traditional and ~~full~~
854 ~~volatile~~full-volatility) for CRACMM and presents the first comprehensive evaluation of PM_{2.5}
855 predictions using the newly developed CRACMM chemical mechanism. The performance of
856 CRACMM with CB6r3_ae7, and Saprc07tic_ae7i are compared, and results demonstrate that
857 CMAQ with CRACMM provides reliable predictions of PM_{2.5} and its components across China
858 during the months of January, April, July, and October 2021, although there are discrepancies
859 in some complex regions.

860 In conclusion, the comparison of the three chemical mechanisms using the traditional POA
861 inventory reveals that differences in R and MB values are generally small. However, with the
862 replacement of the ~~full volatile~~full-volatility inventory, CRACMM tends to predict lower PM_{2.5}
863 concentrations in January across most regions of China except PRD and YRD. In the other
864 months, CRACMM predicts higher concentrations than CB6r3_ae7 and Saprc07tic_ae7i when
865 the ~~full volatile~~full-volatility inventory is incorporated. The differences in PM_{2.5} concentrations
866 in January, are primarily attributed to lower POA concentrations, which are influenced by semi-

设置了格式: 字体: 加粗, 字体颜色: 文字 1

带格式的: 正文

设置了格式: 字体颜色: 文字 1

867 volatile partitioning and reduced aging of semi-volatile POA species under lower temperatures.
868 In contrast, CRACMM simulates elevated SOA concentrations in eastern China due to
869 enhanced precursor availability, while reduced SOA formation is observed in the SCB, where
870 winter conditions slow the oxidation of precursors. The inclusion of the ~~full-volatile~~full-
871 volatility inventory in CRACMM results in higher SOA concentrations in October, driven by
872 increased precursor availability. Overall, CRACMM demonstrates improved performance in
873 terms of R and MB, particularly in January and October for the PRD region, but performs less
874 well in April and July, particularly in the BTH region, compared to CB6r3_ae7. Additionally,
875 CRACMM with the ~~full-volatile~~full-volatility inventory increase in simulated PM_{2.5}
876 concentrations, resulting in smaller deviations from observation across many regions,
877 highlighting the importance of including S/IVOC emissions in the chemical mechanism.
878 Emission perturbation simulations using CMAQ further emphasize the significant role of
879 various emission species, particularly BTX and SVOC, in driving PM_{2.5} formation. The SOA
880 contribution from BTX emissions accounts for nearly 50% of the PM_{2.5} changes, while S/IVOC
881 emissions primarily influence PM_{2.5} through SOA formation. BTX emissions had a more
882 significant impact in CB6r3_ae7, particularly in central China, partly due to the fewer VOC
883 species included in the lumped BTX of the CRACMM mechanism. Future assessments of O₃
884 predictions with CRACMM will offer additional constraints on the gas and aerosol chemistry
885 that contributes to PM_{2.5} formation.

886 **Data availability.** The model simulation is based on the CMAQ v5.4 developed by the U.S.
887 EPA, and the code is publicly available at <https://doi.org/10.5281/zenodo.7218076>. Biogenic
888 emissions were estimated using the MEGANv3.2 model (Guenther et al., 2012b), which is
889 available at <https://bai.ess.uci.edu/megan/data-and-code/megan32>. All input data to reproduce
890 the results and figures in this paper, has been archived on Zenodo
891 ([10.5281/zenodo.18222704](https://doi.org/10.5281/zenodo.18222704)<https://doi.org/10.5281/zenodo.16791307>). (Su and Chen, 2025))
892 and is freely accessible.

893 **Supplement.** The supplement related to this article is available online at

894 **Author contributions.** LL and YJW designed the study. QFS conducted the modeling work,
895 formal analysis and drafted the original manuscript. YFC contributed to data curation and
896 emissions preparation. DCW contributed to model revision, manuscript editing and reviewing.
897 HOTP, GS, BM, BP and YJW provided critical review and editing of the manuscript. LH and
898 YJW contributed to modelling setup. LL supervised the project and secured funding.

带格式的: 行距: 单倍行距

设置了格式: 字体: Times New Roman, 字体颜色: 文字 1

设置了格式: 字体颜色: 文字 1

设置了格式: 字体: Times New Roman, 字体颜色: 文字 1

设置了格式: 字体: (默认) Times New Roman, 字体颜色: 文字 1

设置了格式: 字体: Times New Roman, 字体颜色: 文字 1

设置了格式: 字体颜色: 文字 1

899 **Competing interests.** The authors declare no conflicts of interest.
900 **Disclaimer:** The views expressed in this article are those of the authors and do not necessarily
901 represent the views or the policies of the U.S. ~~Environmental Protection Agency (EPA).~~

902 **Acknowledgements.** This study is financially supported by [Jing-Jin-Ji Regional Integrated](#)
903 [Environmental Improvement-National Science and Technology Major Project \(NO.](#)
904 [2025ZD1202005, 2025ZD1202001\)](#),~~the National Key R&D Program of China~~
905 ~~(2025ZD1202005, 2025ZD1202001, 2025ZD1202004)~~, the National Natural Science
906 Foundation of China (nos. 42375102) and Shanghai International Science and Technology
907 Cooperation Fund (24230740200). This work is supported by the Shanghai Technical Service
908 Center of Science and Engineering Computing, Shanghai University.
909

910 References

- 911 [Boylan, J. W. and Russell, A. G.:](#) PM and light extinction model performance metrics, goals,
912 and criteria for three-dimensional air quality models, *Atmospheric Environment*, 40,
913 4946-4959,doi: <https://doi.org/10.1016/j.atmosenv.2005.09.087>, 2006.
- 914 [Byun, D. and Schere, K. L.:](#) Review of the Governing Equations, Computational Algorithms,
915 and Other Components of the Models-3 Community Multiscale Air Quality (CMAQ)
916 Modeling System, *Applied Mechanics Reviews*, 59, 51-77,doi: 10.1115/1.2128636 %J
917 *Applied Mechanics Reviews*, 2006.
- 918 [Cao, L., Li, S., and Sun, L.:](#) Study of different Carbon Bond 6 (CB6) mechanisms by using a
919 concentration sensitivity analysis, *Atmos. Chem. Phys.*, 21, 12687-12714,doi:
920 10.5194/acp-21-12687-2021, 2021.
- 921 [Carlton, A. G., Bhave, P. V., Napelenok, S. L., Edney, E. O., Sarwar, G., Pinder, R. W.,](#)
922 [Pouliot, G. A., and Houyoux, M.:](#) Model Representation of Secondary Organic Aerosol in
923 CMAQv4.7, *Environ. Sci. Technol.*, 44, 8553-8560,doi: 10.1021/es100636q, 2010.
- 924 [Carter, W.:](#) Implementation Of The Saprc-99 Chemical Mechanism Into The Models-3
925 Framework, 2000.
- 926 [Carter, W. P. L.:](#) DOCUMENTATION OF THE SAPRC-99 CHEMICAL MECHANISM FOR
927 VOC REACTIVITY ASSESSMENT VOLUME 1 OF 2 DOCUMENTATION TEXT,
- 928 [Carter, W. P. L.:](#) Development of the SAPRC-07 chemical mechanism, *Atmos. Environ.*, 44,
929 5324-5335,doi: 10.1016/j.atmosenv.2010.01.026, 2010.
- 930 [Chang, X., Zhao, B., Zheng, H., Wang, S., Cai, S., Guo, F., Gui, P., Huang, G., Wu, D., Han,](#)
931 [L., Xing, J., Man, H., Hu, R., Liang, C., Xu, Q., Qiu, X., Ding, D., Liu, K., Han, R.,](#)
932 [Robinson, A. L., and Donahue, N. M.:](#) Full-volatility emission framework corrects
933 missing and underestimated secondary organic aerosol sources, *One Earth*, 5, 403-
934 412,doi: 10.1016/j.oneear.2022.03.015, 2022.
- 935 [Deng, C., Tian, S., Li, Z., and Li, K.:](#) Spatiotemporal characteristics of PM(2.5) and ozone
936 concentrations in Chinese urban clusters, *Chemosphere*, 295, 133813,doi:
937 10.1016/j.chemosphere.2022.133813, 2022.
- 938 [Derwent, R.:](#) Intercomparison of chemical mechanisms for air quality policy formulation and
939 assessment under North American conditions, *J. Air Waste Manag. Assoc.*, 67, 789-

设置了格式: 字体颜色: 文字 1

940 796,doi: 10.1080/10962247.2017.1292969, 2017.

941 Emery, C., Liu, Z., Russell, A. G., Odman, M. T., Yarwood, G., and Kumar, N.:

942 Recommendations on statistics and benchmarks to assess photochemical model

943 performance, *Journal of the Air & Waste Management Association* (1995), 67, 582-

944 598,doi: 10.1080/10962247.2016.1265027, 2017.

945 Goliff, W. S., Stockwell, W. R., and Lawson, C. V.: The regional atmospheric chemistry

946 mechanism, version 2, *Atmospheric Environment*, 68, 174-185,doi:

947 <https://doi.org/10.1016/j.atmosenv.2012.11.038>, 2013.

948 Gu, J., Chen, Z., Zhang, N., Peng, S., Cui, W., Huo, G., and Chen, F.: Characterization of

949 Atmospheric Fine Particles and Secondary Aerosol Estimated under the Different

950 Photochemical Activities in Summertime Tianjin, China, *International journal of*

951 *environmental research and public health*, 19,doi: 10.3390/ijerph19137956, 2022.

952 Guenther, A. B., Jiang, X., Heald, C. L., Sakulyanontvittaya, T., Duhl, T., Emmons, L. K., and

953 Wang, X.: The Model of Emissions of Gases and Aerosols from Nature version 2.1

954 (MEGAN2.1): an extended and updated framework for modeling biogenic emissions,

955 *Geosci. Model Dev.*, 5, 1471-1492,doi: 10.5194/gmd-5-1471-2012, 2012.

956 Harrison, R. M., Beddows, D. C. S., Tong, C., and Damayanti, S.: Non-linearity of secondary

957 pollutant formation estimated from emissions data and measured precursor-secondary

958 pollutant relationships, *npj Climate and Atmospheric Science*, 5, 71,doi: 10.1038/s41612-

959 022-00297-9, 2022.

960 Huang, L., Wang, Q., Wang, Y., Emery, C., Zhu, A., Zhu, Y., Yin, S., Yarwood, G., Zhang, K.,

961 and Li, L.: Simulation of secondary organic aerosol over the Yangtze River Delta region:

962 The impacts from the emissions of intermediate volatility organic compounds and the

963 SOA modeling framework, *Atmospheric Environment*, 246, 118079,doi:

964 <https://doi.org/10.1016/j.atmosenv.2020.118079>, 2021a.

965 Huang, L., Zhu, Y., Zhai, H., Xue, S., Zhu, T., Shao, Y., Liu, Z., Emery, C., Yarwood, G.,

966 Wang, Y., Fu, J., Zhang, K., and Li, L.: Recommendations on benchmarks for numerical

967 air quality model applications in China – Part 1: PM_{2.5} and chemical species, *Atmos.*

968 *Chem. Phys.*, 21, 2725-2743,doi: 10.5194/acp-21-2725-2021, 2021b.

969 Huang, L., Wu, Z. a., Liu, H., Yarwood, G., Huang, D., Wilson, G., Chen, H., Ji, D., Tao, J.,

970 Han, Z., Wang, Y., Wang, H., Huang, C., and Li, L.: An improved framework for

971 efficiently modeling organic aerosol (OA) considering primary OA evaporation and

972 secondary OA formation from VOCs, IVOCs, and SVOCs, *Environmental Science:*

973 *Atmospheres*,doi: 10.1039/d4ea00060a, 2024.

974 Huo, Q., Yin, Z., Ma, X., and Wang, H.: Distinctive dust weather intensities in North China

975 resulted from two types of atmospheric circulation anomalies, *Atmos. Chem. Phys.*, 25,

976 1711-1724,doi: 10.5194/acp-25-1711-2025, 2025.

977 Kang, M., Zhang, H., and Ying, Q.: Effectiveness of emission controls on atmospheric

978 oxidation capacity and air pollutant concentrations: uncertainties due to chemical

979 mechanisms and inventories, *Atmos. Chem. Phys.*, 25, 11453-11467,doi: 10.5194/acp-25-

980 11453-2025, 2025.

981 Kang, M., Hu, J., Zhang, H., and Ying, Q.: Evaluation of a highly condensed SAPRC

982 chemical mechanism and two emission inventories for ozone source apportionment and

983 emission control strategy assessments in China, *Sci. Total Environ.*, 813, 151922,doi:

984 10.1016/j.scitotenv.2021.151922, 2022.

985 Kang, Y.-H., Oh, I., Jeong, J.-H., Bang, J.-H., Kim, Y.-K., Kim, S., Kim, E., Hong, J.-H., and
986 Lee, D.-G. J. J. o. E. S. I.: Comparison of CMAQ ozone simulations with two chemical
987 mechanisms (SAPRC99 and CB05) in the Seoul metropolitan region, 25, 85-97, 2016.

988 Kim, K.-H., Kabir, E., and Kabir, S.: A review on the human health impact of airborne
989 particulate matter, *Environment International*, 74, 136-143,doi:
990 <https://doi.org/10.1016/j.envint.2014.10.005>, 2015.

991 Koo, B., Knipping, E., and Yarwood, G.: 1.5-Dimensional volatility basis set approach for
992 modeling organic aerosol in CAMx and CMAQ, *Atmos. Environ.*, 95, 158-164,doi:
993 10.1016/j.atmosenv.2014.06.031, 2014.

994 Liu, J., Niu, X., Zhang, L., Yang, X., Zhao, P., and He, C.: Exposure risk assessment and
995 synergistic control pathway construction for O₃-PM_{2.5} compound pollution in China,
996 *Atmospheric Environment: X*, 21, 100240,doi:
997 <https://doi.org/10.1016/j.aeaoa.2024.100240>, 2024.

998 Luecken, D. J., Yarwood, G., and Hutzell, W. T.: Multipollutant modeling of ozone, reactive
999 nitrogen and HAPs across the continental US with CMAQ-CB6, *Atmos. Environ.*, 201,
1000 62-72,doi: 10.1016/j.atmosenv.2018.11.060, 2019.

1001 Mao, J., Li, L., Li, J., Sulaymon, I. D., Xiong, K., Wang, K., Zhu, J., Chen, G., Ye, F., Zhang,
1002 N., Qin, Y., Qin, M., and Hu, J.: Evaluation of Long-Term Modeling Fine Particulate
1003 Matter and Ozone in China During 2013–2019, Volume 10 - 2022,doi:
1004 10.3389/fenvs.2022.872249, 2022.

1005 Meng, F., Du, X., Tang, W., He, J., Li, Y., Wang, X., Yu, S., Tang, X., Xing, J., Xie, M., Zeng,
1006 L., and Dong, H.: Evaluation of Regional Atmospheric Models for Air Quality
1007 Simulations in the Winter Season in China, *Atmosphere*, 17, 1,doi:
1008 10.3390/atmos17010001, 2026.

1009 Murphy, B. N., Woody, M. C., Jimenez, J. L., Carlton, A. M. G., Hayes, P. L., Liu, S., Ng, N.
1010 L., Russell, L. M., Setyan, A., Xu, L., Young, J., Zaveri, R. A., Zhang, Q., and Pye, H. O.
1011 T.: Semivolatile POA and parameterized total combustion SOA in CMAQv5.2: impacts
1012 on source strength and partitioning, *Atmos. Chem. Phys.*, 17, 11107-11133,doi:
1013 10.5194/acp-17-11107-2017, 2017.

1014 Murray, C. J. L., Aravkin, A. Y., and Zheng, P.: Global burden of 87 risk factors in 204
1015 countries and territories, 1990–2019: a systematic analysis for the Global Burden
1016 of Disease Study 2019, *The Lancet*, 396, 1223-1249,doi: 10.1016/S0140-6736(20)30752-
1017 2, 2020.

1018 Ng, N. L., Kwan, A. J., Surratt, J. D., Chan, A. W. H., Chhabra, P. S., Sorooshian, A., Pye, H.
1019 O. T., Crounse, J. D., Wennberg, P. O., Flagan, R. C., and Seinfeld, J. H.: Secondary
1020 organic aerosol (SOA) formation from reaction of isoprene with nitrate radicals (NO₃),
1021 *Atmospheric Chemistry and Physics*, 8, 4117-4140,doi: 10.5194/acp-8-4117-2008, 2008.

1022 Otte, T. L. and Pleim, J. E.: The Meteorology-Chemistry Interface Processor (MCIP) for the
1023 CMAQ modeling system: updates through MCIPv3.4.1, *Geosci. Model Dev.*, 3, 243-
1024 256,doi: <http://10.5194/gmd-3-243-2010>, 2010.

1025 Place, B. K., Hutzell, W. T., Appel, K. W., Farrell, S., Valin, L., Murphy, B. N., Seltzer, K. M.,
1026 Sarwar, G., Allen, C., Piletic, I. R., D'Ambro, E. L., Saunders, E., Simon, H., Torres-
1027 Vasquez, A., Pleim, J., Schwantes, R. H., Coggon, M. M., Xu, L., Stockwell, W. R., and

1028 Pye, H. O. T.: Sensitivity of northeastern US surface ozone predictions to the
1029 representation of atmospheric chemistry in the Community Regional Atmospheric
1030 Chemistry Multiphase Mechanism (CRACMMv1.0), *Atmos. Chem. Phys.*, 23, 9173-
1031 9190,doi: 10.5194/acp-23-9173-2023, 2023a.

1032 Place, B. K., Hutzell, W. T., Appel, K. W., Farrell, S., Valin, L., Murphy, B. N., Seltzer, K. M.,
1033 Sarwar, G., Allen, C., Piletic, I. R., D'Ambro, E. L., Saunders, E., Simon, H., Torres-
1034 Vasquez, A., Pleim, J., Schwantes, R. H., Coggon, M. M., Xu, L., Stockwell, W. R., and
1035 Pye, H. O. T.: Sensitivity of northeastern US surface ozone predictions to the
1036 representation of atmospheric chemistry in the Community Regional Atmospheric
1037 Chemistry Multiphase Mechanism (CRACMMv1.0), *Atmospheric Chemistry and
1038 Physics*, 23, 9173-9190,doi: 10.5194/acp-23-9173-2023, 2023b.

1039 Pye, H. O. T. and Pouliot, G. A.: Modeling the Role of Alkanes, Polycyclic Aromatic
1040 Hydrocarbons, and Their Oligomers in Secondary Organic Aerosol Formation, *Environ.
1041 Sci. Technol.*, 46, 6041-6047,doi: 10.1021/es300409w, 2012.

1042 Pye, H. O. T., Luecken, D. J., Xu, L., Boyd, C. M., Ng, N. L., Baker, K. R., Ayres, B. R.,
1043 Bash, J. O., Baumann, K., Carter, W. P. L., Edgerton, E., Fry, J. L., Hutzell, W. T.,
1044 Schwede, D. B., and Shepson, P. B.: Modeling the Current and Future Roles of
1045 Particulate Organic Nitrates in the Southeastern United States, *Environ. Sci. Technol.*, 49,
1046 14195-14203,doi: 10.1021/acs.est.5b03738, 2015a.

1047 Pye, H. O. T., Luecken, D. J., Xu, L., Boyd, C. M., Ng, N. L., Baker, K. R., Ayres, B. R.,
1048 Bash, J. O., Baumann, K., Carter, W. P. L., Edgerton, E., Fry, J. L., Hutzell, W. T.,
1049 Schwede, D. B., and Shepson, P. B.: Modeling the Current and Future Roles of
1050 Particulate Organic Nitrates in the Southeastern United States, *Environmental Science &
1051 Technology*, 49, 14195-14203,doi: 10.1021/acs.est.5b03738, 2015b.

1052 Pye, H. O. T., Pinder, R. W., Piletic, I. R., Xie, Y., Capps, S. L., Lin, Y.-H., Surratt, J. D.,
1053 Zhang, Z., Gold, A., Luecken, D. J., Hutzell, W. T., Jaoui, M., Offenberg, J. H.,
1054 Kleindienst, T. E., Lewandowski, M., and Edney, E. O.: Epoxide Pathways Improve
1055 Model Predictions of Isoprene Markers and Reveal Key Role of Acidity in Aerosol
1056 Formation, *Environ. Sci. Technol.*, 47, 11056-11064,doi: 10.1021/es402106h, 2013.

1057 Pye, H. O. T., Murphy, B. N., Xu, L., Ng, N. L., Carlton, A. G., Guo, H., Weber, R., Vasilakos,
1058 P., Appel, K. W., Budisulistiorini, S. H., Surratt, J. D., Nenes, A., Hu, W., Jimenez, J. L.,
1059 Isaacman-VanWertz, G., Misztal, P. K., and Goldstein, A. H.: On the implications of
1060 aerosol liquid water and phase separation for organic aerosol mass, *Atmos. Chem. Phys.*,
1061 17, 343-369,doi: 10.5194/acp-17-343-2017, 2017.

1062 Pye, H. O. T., Place, B. K., Murphy, B. N., Seltzer, K. M., D'Ambro, E. L., Allen, C., Piletic,
1063 I. R., Farrell, S., Schwantes, R. H., Coggon, M. M., Saunders, E., Xu, L., Sarwar, G.,
1064 Hutzell, W. T., Foley, K. M., Pouliot, G., Bash, J., and Stockwell, W. R.: Linking gas,
1065 particulate, and toxic endpoints to air emissions in the Community Regional Atmospheric
1066 Chemistry Multiphase Mechanism (CRACMM), *Atmospheric Chemistry and Physics*, 23,
1067 5043-5099,doi: 10.5194/acp-23-5043-2023, 2023a.

1068 Pye, H. O. T., Place, B. K., Murphy, B. N., Seltzer, K. M., D'Ambro, E. L., Allen, C., Piletic,
1069 I. R., Farrell, S., Schwantes, R. H., Coggon, M. M., Saunders, E., Xu, L., Sarwar, G.,
1070 Hutzell, W. T., Foley, K. M., Pouliot, G., Bash, J., and Stockwell, W. R.: Linking gas,
1071 particulate, and toxic endpoints to air emissions in the Community Regional Atmospheric

1072 Chemistry Multiphase Mechanism (CRACMM), *Atmos. Chem. Phys.*, 23, 5043-
1073 5099, doi: 10.5194/acp-23-5043-2023, 2023b.

1074 Robinson, A. L., Donahue, N. M., Shrivastava, M. K., Weitkamp, E. A., Sage, A. M.,
1075 Grieshop, A. P., Lane, T. E., Pierce, J. R., and Pandis, S. N.: Rethinking Organic
1076 Aerosols: Semivolatile Emissions and Photochemical Aging, *Science*, 315, 1259-
1077 1262, doi: 10.1126/science.1133061, 2007.

1078 Sarwar, G., Luecken, D., Yarwood, G., Whitten, G. Z., Carter, W. P. J. J. o. a. m., and
1079 climatology: Impact of an updated carbon bond mechanism on predictions from the
1080 CMAQ modeling system: Preliminary assessment, 47, 3-14, 2008.

1081 Seinfeld, J. H., Pandis, S. N. J. A. c., and physics: From air pollution to climate change, 1326,
1082 1998.

1083 Skamarock, W. C., Klemp, J., Dudhia, J., Gill, D. O., Liu, Z., and Berner, J.: A Description
1084 of the Advanced Research WRF Model Version 4, doi: <https://doi.org/10.5065/1dfh-6p97>,
1085 2019.

1086 Skipper, T. N., D'Ambro, E. L., Wiser, F. C., McNeill, V. F., Schwantes, R. H., Henderson, B.
1087 H., Piletic, I. R., Baublitz, C. B., Bash, J. O., Whitehill, A. R., Valin, L. C., Mouat, A. P.,
1088 Kaiser, J., Wolfe, G. M., St. Clair, J. M., Hanisco, T. F., Fried, A., Place, B. K., and Pye,
1089 H. O. T.: Role of chemical production and depositional losses on formaldehyde in the
1090 Community Regional Atmospheric Chemistry Multiphase Mechanism (CRACMM),
1091 *Atmospheric Chemistry and Physics*, 24, 12903-12924, doi: 10.5194/acp-24-12903-2024,
1092 2024.

1093 Stockwell, W. R., Lawson, C. V., Saunders, E., and Goliff, W. S.: A Review of Tropospheric
1094 Atmospheric Chemistry and Gas-Phase Chemical Mechanisms for Air Quality Modeling,
1095 *Atmosphere*, 3, 1-32, doi: 10.3390/atmos3010001, 2012.

1096 Su, Q. and Chen, Y.: Zenodo [data set], doi: 10.5281/zenodo.18222704, 2025.

1097 Tsai, Y. G., Wang, J. Y., Yang, K. D., Yang, H. Y., Yeh, Y. P., Chang, Y. J., Lee, J. H., Wang, S.
1098 L., Huang, S. K., and Chan, C. C.: Long-term PM(2.5) exposure impairs lung growth and
1099 increases airway inflammation in Taiwanese school children, *ERJ open research*, 11, doi:
1100 10.1183/23120541.00972-2024, 2025.

1101 Wang, Y., Pavuluri, C. M., Fu, P., Li, P., Dong, Z., Xu, Z., Ren, H., Fan, Y., Li, L., Zhang, Y.-
1102 L., and Liu, C.-Q.: Characterization of Secondary Organic Aerosol Tracers over Tianjin,
1103 North China during Summer to Autumn, *ACS Earth and Space Chemistry*, 3, 2339-
1104 2352, doi: 10.1021/acsearthspacechem.9b00170, 2019.

1105 Wang, Y., Ning, M., Su, Q., Wang, L., Jiang, S., Feng, Y., Wu, W., Tang, Q., Hou, S., Bian, J.,
1106 Huang, L., Lu, G., Manomaiphiboon, K., Kaynak, B., Zhang, K., Chen, H., and Li, L.:
1107 Designing regional joint prevention and control schemes of PM2.5 based on source
1108 apportionment of chemical transport model: A case study of a heavy pollution episode, *J.*
1109 *Clean. Prod.*, 455, 142313, doi: 10.1016/j.jclepro.2024.142313, 2024.

1110 Wong, D. C., Willison, J., Pleim, J. E., Sarwar, G., Beidler, J., Bullock, R., Herwehe, J. A.,
1111 Gilliam, R., Kang, D., Hogrefe, C., Pouliot, G., and Foroutan, H.: Development of the
1112 MPAS-CMAQ coupled system (V1.0) for multiscale global air quality modeling, *Geosci.*
1113 *Model Dev.*, 17, 7855-7866, doi: 10.5194/gmd-17-7855-2024, 2024.

1114 Woody, M. C., Baker, K. R., Hayes, P. L., Jimenez, J. L., Koo, B., and Pye, H. O. T.:
1115 Understanding sources of organic aerosol during CalNex-2010 using the CMAQ-VBS,

1116 Atmos. Chem. Phys., 16, 4081-4100,doi: 10.5194/acp-16-4081-2016, 2016.
1117 Xie, Y., Paulot, F., Carter, W. P. L., Nolte, C. G., Luecken, D. J., Hutzell, W. T., Wennberg, P.
1118 O., Cohen, R. C., and Pinder, R. W.: Understanding the impact of recent advances in
1119 isoprene photooxidation on simulations of regional air quality, Atmos. Chem. Phys., 13,
1120 8439-8455,doi: 10.5194/acp-13-8439-2013, 2013.
1121 Yarwood, G., Morris, R. E., and Wilson, G. M.: Particulate Matter Source Apportionment
1122 Technology (PSAT) in the CAMx Photochemical Grid Model, Air Pollution Modeling
1123 and Its Application XVII, Boston, MA, 2007//, 478-492,
1124 Yarwood, G., Rao, S., Yocke, M., and Whitten, G.: Updates to the carbon bond chemical
1125 mechanism: CB05 final report to the US EPA, RT-0400675, 2005.
1126 Yarwood, G., Jung, J., Whitten, G. Z., Heo, G., Mellberg, J., and Estes, M.: UPDATES TO
1127 THE CARBON BOND MECHANISM FOR VERSION 6 (CB6),
1128 Zhang, J., He, X., Ding, X., Yu, J. Z., and Ying, Q.: Modeling Secondary Organic Aerosol
1129 Tracers and Tracer-to-SOA Ratios for Monoterpenes and Sesquiterpenes Using a
1130 Chemical Transport Model, Environmental Science & Technology, 56, 804-813,doi:
1131 10.1021/acs.est.1c06373, 2022.
1132 Zhang, J., He, X., Gao, Y., Zhu, S., Jing, S., Wang, H., Yu, J. Z., and Ying, Q.: Estimation of
1133 Aromatic Secondary Organic Aerosol Using a Molecular Tracer—A Chemical Transport
1134 Model Assessment, Environ. Sci. Technol.,doi: 10.1021/acs.est.1c03670, 2021a.
1135 Zhang, J., He, X., Gao, Y., Zhu, S., Jing, S., Wang, H., Yu, J. Z., and Ying, Q.: Assessing
1136 Regional Model Predictions of Wintertime SOA from Aromatic Compounds and
1137 Monoterpenes with Precursor-specific Tracers, Aerosol and Air Quality Research, 21,doi:
1138 10.4209/aaqr.210233, 2021b.
1139 Zhang, J., Liu, J., Ding, X., He, X., Zhang, T., Zheng, M., Choi, M., Isaacman-VanWertz, G.,
1140 Yee, L., Zhang, H., Misztal, P., Goldstein, A. H., Guenther, A. B., Budisulistiorini, S. H.,
1141 Surratt, J. D., Stone, E. A., Shrivastava, M., Wu, D., Yu, J. Z., and Ying, Q.: New
1142 formation and fate of Isoprene SOA markers revealed by field data-constrained modeling,
1143 npj Climate and Atmospheric Science, 6, 69,doi: 10.1038/s41612-023-00394-3, 2023.
1144 Zhu, S., Wang, Z., Qu, K., Xu, J., Zhang, J., Yang, H., Wang, W., Sui, X., Wei, M., and Liu,
1145 H.: Spatial Characteristics and Influence of Topography and Synoptic Systems on PM2.5
1146 in the Eastern Monsoon Region of China, Aerosol and Air Quality Research, 23,
1147 220393,doi: 10.4209/aaqr.220393, 2023.

1148

设置了格式: 字体颜色: 文字 1